October 1969
Max J. Miller

DEVIATION ANGLE PREDICTION METHODS —A REVIEW

TURBOMACHINERY
COMPONENTS RESEARCH PROGRAM

Interim Report for National Aeronautics and Space Administration
Grant ~~44-002-005~~ NGL-16-002-00

ERI-560 Project 407-S

ENGINEERING RESEARCH INSTITUTE
IOWA STATE UNIVERSITY
AMES, IOWA 50010 USA

ENGINEERING RESEARCH

ENGINEERING RESEARCH
ENGINEERING RESEARCH
ENGINEERING RESEARCH
ENGINEERING RESEARCH

DEVIATION ANGLE PREDICTION METHODS—A REVIEW

Max J. Miller

October 1969

Interim Report for National
Aeronautics and Space Administration
Grant 16-002-005

ERI-580
Project 407-S

ENGINEERING RESEARCH INSTITUTE
IOWA STATE UNIVERSITY AMES

DEVIATION ANGLE PREDICTION METHODS – A REVIEW

Max J. Miller

ABSTRACT

Predicting the direction of flow leaving an annular cascade of blades is a key problem in axial-flow turbomachinery. This report is a review of methods which have been proposed for the prediction of deviation angles in axial-flow pumps and compressors. A large number of variables influence deviation angle, however methods of predicting the effects of many variables have not been published, hence this review was limited to the effects of

- two-dimensional geometric parameters
- incidence angle
- axial velocity ratio
- secondary flow
- sweep and dihedral.

CONTENTS

INTRODUCTION

Predicting the direction of flow leaving an annular cascade of blades is a key problem in axial-flow turbomachinery. In the design problem, blades must be selected which will produce a prescribed fluid velocity, pressure, and angle distribution at the exit of the blade row for specified inlet flow conditions. In the performance prediction problem or analysis problem, blade geometry is prescribed and for given inlet flow conditions the outlet flow conditions must be computed. Solutions to both problems are often obtained using the blade-element method in which flow is assumed to be axisymmetric (i.e. no gradients in the tangential direction), stream surfaces are assumed to be conical and the flow conditions are computed at stations between blade rows. The flow is assumed steady and local viscous effects are neglected although cumulative viscous effects are included in the solution in the form of total pressure loss between computing stations.

In the usual formulation of the blade-element method for the design problem, the exit flow conditions and in particular the average flow angles are computed from an estimated distribution of total pressure loss and a specified distribution of another parameter such as energy addition or pressure ratio. Blade sections must then be selected to produce the desired average flow angles at each radius. The blade sections chosen must reflect the fact that the average angle of the leaving flow is not parallel to the outlet blade angle (the tangent to the blade section mean line at the trailing edge). The discrepancy between the average leaving flow angle and the outlet blade angle is defined as the deviation angle (Fig. 1) and must be estimated to complete the blade-section specification.

In a blade-element method solution of the analysis problem, estimates of

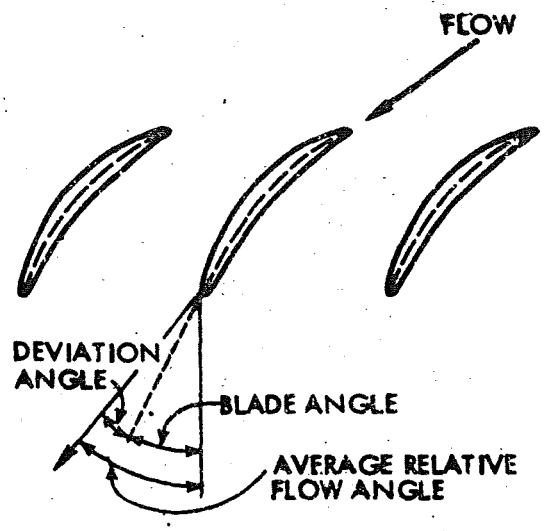

Figure 1 – Flow deviation angle in a cascade of blades. (See nomenclature for definition of blade and flow angle.)

the deviation angle and total pressure loss for a number of blade sections along the span, the equation of motion in the radial direction, and the continuity equation are sufficient to compute the exit flow conditions. Both accurate design and performance prediction thus depend on accurate prediction of deviation angle.

This report is a review of methods which have been proposed for the prediction of deviation angles in axial-flow pumps and compressors. The methods are discussed from a blade-element approach, and only incompressible and low-speed compressible flow (essentially constant density flow) are considered. The review is divided into sections dealing with parameters and phenomena which are recognized to influence deviation angle. The various parameters included are not considered to be independent and in fact some are probably quite interdependent. A large number of variables which influence deviation angle, given by Serovy (Ref. 1), are listed in the Appendix. Because of inadequate experimental information or because a theoretical analysis is too difficult, no quantitative methods have been developed to predict the effects of many of these variables on deviation angle. Because of this it was decided to limit this review to the effects of

- two-dimensional geometric parameters
- incidence angle
- axial velocity ratio

- secondary flow
- sweep and dihedral

for which quantitative methods have been published. With a few exceptions, only references written in English are given. In sections such as Secondary Flow where a very large amount of work has been published no attempt was made to include all applicable references, but instead representative and significant papers were reviewed.

CASCADE NOMENCLATURE

General cascade notation used throughout this report is defined in this section. Specialized definitions are given in the sections where they are used. All symbols are defined in the symbol list.

A meridional view of an axial flow rotor is shown in Figure 2. If the

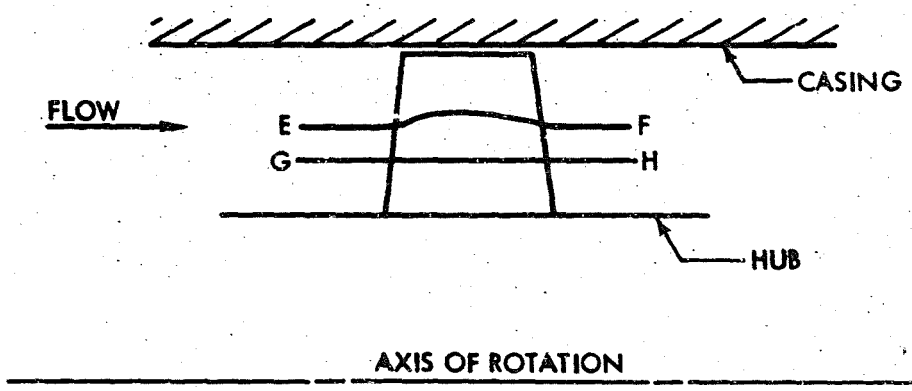

Figure 2 — Meridional plane view of an axial-flow rotor.

flow is assumed to be axixymmetric, then a typical streamline EF can be revolved intc the meridional plane. The surface developed by rotating the streamline about the axis of rotation is called an axisymmetric stream surface. The axisymmetric stream surface is often assumed to be conical if

computation stations are between blade rows, but it usually is not conical if computation stations also are placed inside the blade row. If the cylindrical stream surface corresponding to GH in Figure 2 is developed with the blade intersections shown, a view similar to Figure 3 results. Blade parameters and

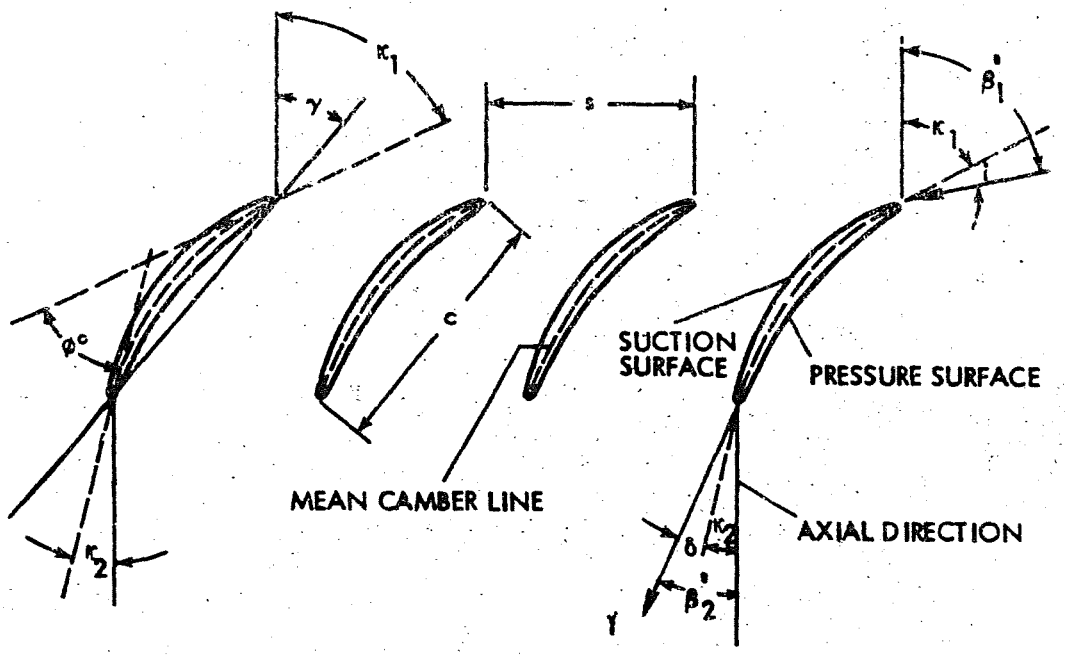

Figure 3 -- Two-dimensional cascade view and blade nomenclature.

their relationships to the flow relative velocity vectors are defined schematically in Figure 3. The blade chord, c, is defined as the line connecting the end points of the mean camber line. The angle between the chord line and the axial direction is the blade stagger angle, γ. Blade angles, κ_1 and κ_2, are defined as the angle between the axial direction and the tangent to the blade mean line at the leading and trailing edges. The relative

flow angles, β_1', β_2', are blade-to-blade average values (ideally mass-averaged values) of the flow angles measured in a coordinate system fixed to blades. A typical blade-to-blade distribution of flow angle is shown in Figure 4.

Deviation angle, δ, is the difference between the average leaving relative flow angle, β_2', and the blade angle, κ_2, as shown in Figure 3.

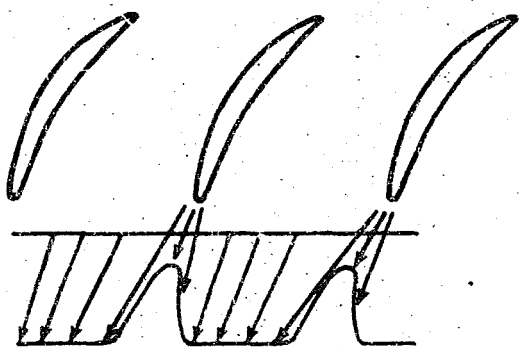

Figure 4 — Blade-to-blade variation of relative flow angle.

TWO-DIMENSIONAL GEOMETRIC PARAMETERS

Ultimately, the deviation angle distribution in an annular cascade, rotating or stationary, is determined (for a given fluid, flow rate, and rotational speed) by the geometric shape and arrangement of the blades and the boundaries at the hub and tip. To consider the problem in its full three-dimensional form would be a formidable task and accordingly simplifying approximations have been sought. The problem has been reduced to a two-dimensional problem by assuming that the deviation angle is determined by the geometric parameters of the blade sections cut by an axisymmetric stream surface and is not dependent on the blade geometry at other positions along the span. Two-dimensional cascade results and to a lesser extent potential flow have been used to establish the values of deviation angle for various two-dimensional cascade geometries. The plausibility of the dependence of deviation angle in two-dimensional flow on geometric parameters can be established by considering the cascades drawn in Figure 5. The cascades in Figure 5a each have the same chord, solidity, and

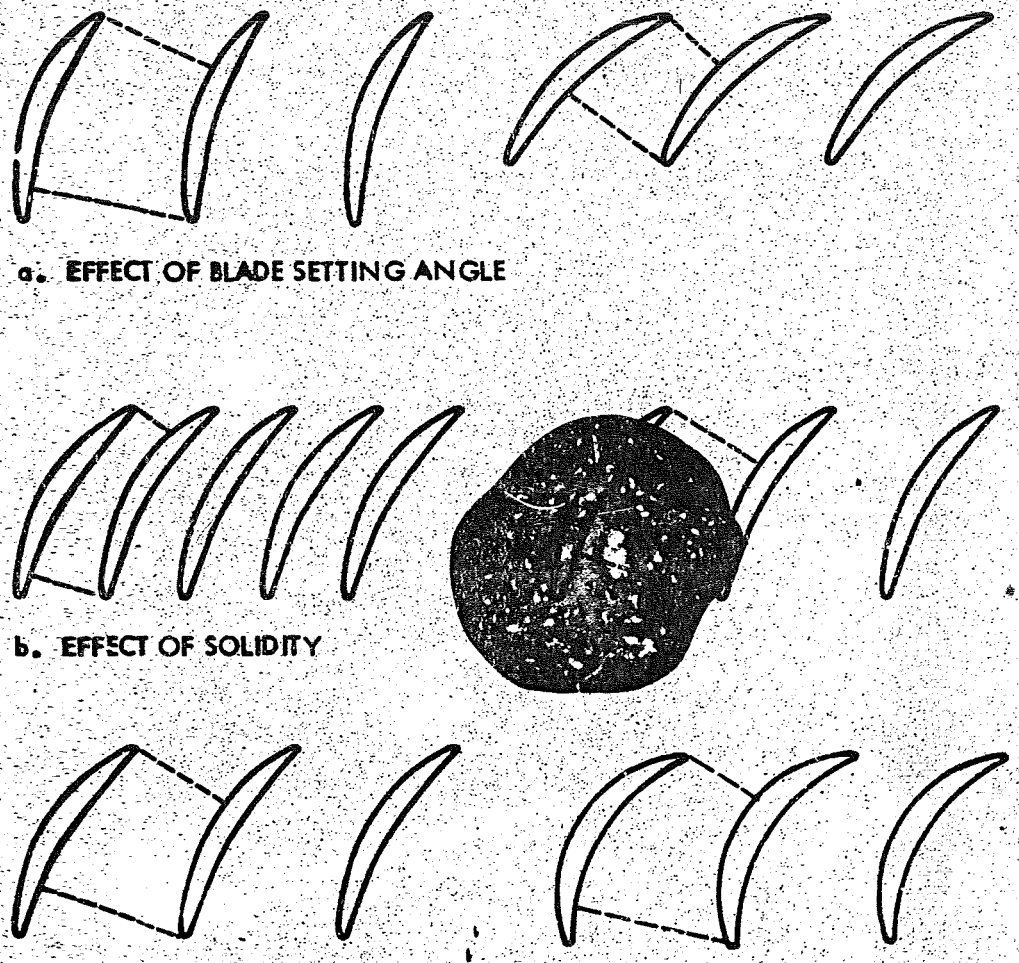

Figure 5 — Effect of geometric parameters on deviation angle.

camber, but the cascade on the right has a higher blade stagger angle than the other cascade and hence has a significantly shorter length of passage which is bounded on both sides by blade surface. Thus, for a given incidence angle, increasing stagger angle tends to decrease guidance of the flow and hence tends to increase deviation angle. Decreasing solidity, σ, also tends to decrease guidance of the flow and increase deviation angle as seen by the

difference in channel length of the two cascades in Figure 5b. Although it is not so graphically obvious, (Fig. 5c) deviation angle does increase with increasing camber, and according to Lieblein (Ref. 2) the relationship between deviation angle and camber is linear for potential flow. Other parameters such as blade thickness distribution, camber line shape, surface finish, and trailing edge radius usually have less influence on deviation angle than camber, solidity, and blade setting angle.

Consequently, an early deviation angle prediction method, called Carter's rule, expresses deviation angle as

$$\delta = \frac{m_c \theta}{\sigma^{\frac{1}{2}}} \qquad (1)$$

where m_c is a function of blade setting angle and the position of maximum camber. Curves of m_c as a function of blade setting angle are given in Carter and Hughes (Ref. 3) for circular arc and parabolic arc (maximum camber at 40 percent of the chord from the leading edge) camberline blades. These curves were deduced from both theoretical and experimental results. For accelerating cascades the exponent on solidity should be unity rather than one-half according to Carter (Ref. 4). Howell (Ref. 5) ascribed to Constant (Ref. 6) an early version of Equation (1) in which $m_c = 0.26$ was used. Equation (1) applies specifically to the "nominal" incidence angle which Howell (Ref. 5) defines as the incidence angle for which the turning angle, $(\beta_1' - \beta_2')$, is equal to 0.8 of the turning angle at which the loss is twice the minimum value; however it is frequently applied throughout the low-loss incidence angle range (defined in the Incidence Angle Section) under the assumption that deviation angle does not change appreciably with incidence angle in the low-loss range.

A deviation angle prediction method which includes more geometric

parameters was presented by Lieblein (Ref. 2). The method was based on correlations of two-dimensional cascade data for NACA 65-series compressor blades which were presented by Emery, et al. (Ref. 7). The correlations were made for operation at a reference incidence angle defined to be midway between the incidence angles at which the total pressure loss across the cascade was equal to twice the minimum-loss value (see Fig. 6). At the

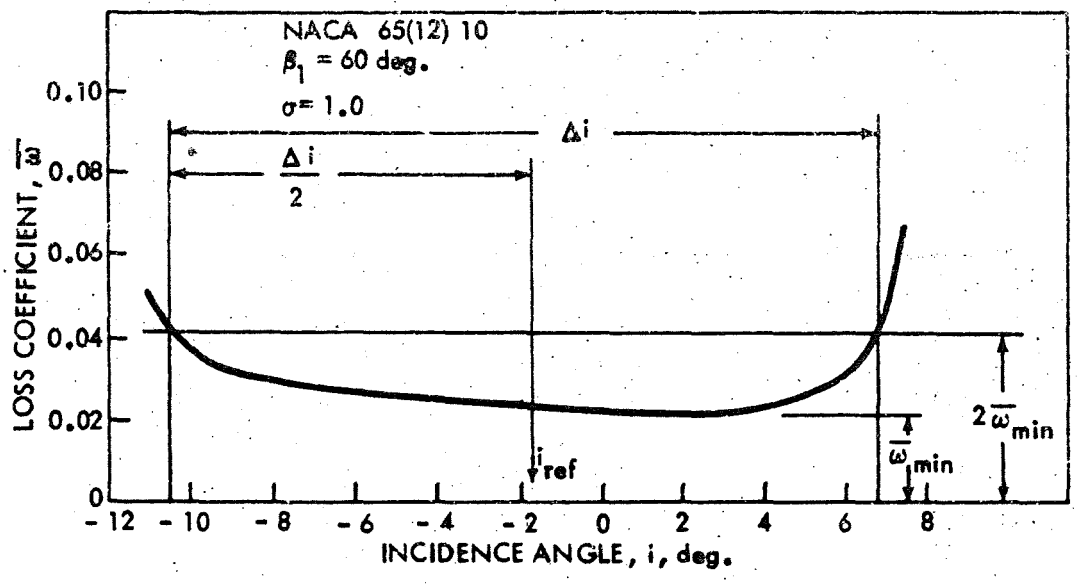

Figure 6 — Schematic definition of refer ce incidence angle. Data from Reference 7.

reference incidence angle, deviation angle is expressed as

$$\delta = \delta_o + m\phi^\circ \tag{2}$$

where δ_o is the reference deviation angle for zero camber, ϕ° is camber, and m is the slope of the deviation angle function with camber. Curves are presented by Lieblein (Ref. 2) giving the slope factor m as a function of

inlet air angle and solidity for circular-arc-mean-line blades. Inlet air angle was used instead of blade stagger angle because the cascade data of Emery, et al. (Ref. 7) were obtained at a constant inlet air angle rather than a constant blade stagger angle. The zero-camber deviation angle is given by Lieblein (Ref. 2) as

$$\delta_o = (K_\delta)_{sh}(K_\delta)_t(\delta_o)_{10} \tag{3}$$

where $(\delta_o)_{10}$ represents the zero-camber deviation angle for a 10-percent-thick NACA 65-series distribution, $(K_\delta)_{sh}$ is a correction for blade shapes with thickness distributions different from the 65-series, and $(K_\delta)_t$ is a correction for maximum blade thickness other than 10 percent of the chord. Empirical curves are given for $(\delta_o)_{10}$ as a function of inlet air angle and solidity and for $(K_\delta)_t$ as a function of maximum thickness ratio, t_{max}/c. A value of 1.1 for $(K_\delta)_{sh}$ is recommended for C-series circular-arc blades and 0.7 for double-circular-arc blades. Both of these values are based on limited data. Plots of deviation angle versus camber comparing values from Equation (2) with cascade data of Emery, et al. (Ref. 7) are given by Lieblein (Ref. 2). The linear curves from Equation (3) approximate the data quite well. However, at high cambers where D-factors exceed 0.62, the experimental data tends to fall above the predicted values. D-factor is used as a measure of blade loading and was developed by Lieblein, et al. (Ref. 8). Blade sections operating at D-factors greater than 0.62 evidently have blade surface boundary layers thick enough at i_{ref} to cause the flow to differ significantly from potential flow where a linear relation between deviation angle and camber angle is predicted. A quantitative evaluation of deviation angle as a function of camber for D-factors greater than 0.62 is currently lacking, and is an area where further research effort could make a significant contribution to axial-flow pump and compressor technology.

Both methods described in this section assumed the incidence angle to be fixed at some "design" value. In the following section, methods to predict the deviation angle at "off-design" values of incidence angle are reviewed.

INCIDENCE ANGLE

Plane Cascades

The deviation angle of a plane cascade is a function of the incidence angle and blade geometry. A typical curve of deviation angle as a function of incidence angle for a cascade with a fixed inlet flow angle is shown in Figure 7. The deviation angle curve can be roughly divided into two parts, one corresponding to the so-called low-loss incidence angle interval and the other corresponding to incidence angles outside the low-loss interval. When the incidence angle is in the low-loss interval, the blade surface boundary layers are probably quite thin so that the flow closely approximates potential flow. Therefore in the low-loss region, the functional relationship between deviation angle and incidence angle for a two-dimensional cascade is quite similar to the relationship for potential flow. Lieblein (Ref. 9) concluded, based on calculations using the potential flow theory of Weinig (Ref. 10), that $d\delta/di$ is positive for potential flow and that it is a function of solidity and blade chord angle. Smith (Ref. 11), in a discussion of Reference 9, indicated that $d\delta/di$ is also a strong function of camber.

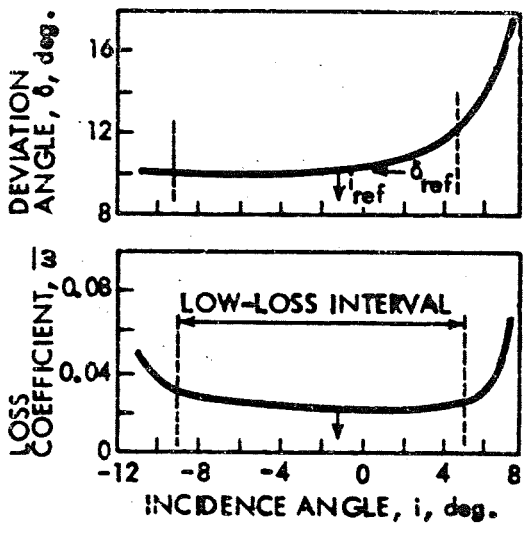

Figure 7 — Typical cascade results.

Using the low-speed cascade data for 65-(A_{10}) 10 blades of Reference 7, Lieblein developed an empirical method to estimate the variation of deviation angle in the low-loss incidence interval. He assumed that since operation could be considered to be in the low-loss region for only a small incidence angle interval, the following linear function could be used to compute deviation angle:

$$\delta = \delta_{ref} + (i - i_{ref}) \left(\frac{d\delta}{di}\right)_{ref} \tag{4}$$

where i_{ref} is the reference incidence angle as defined in the Two-Dimensional Geometric Parameters section above, δ_{ref} is the measured deviation angle at $i = i_{ref}$, and $(d\delta/di)_{ref}$ is the graphically determined slope of the deviation angle curve at $i = i_{ref}$. Lieblein presented a family of curves from which values of $(d\delta/di)_{ref}$ may be obtained for solidities ranging from 0 to 1.8 and for inlet air angles ranging from 0 to 70 degrees. These correlations are also presented in Reference 2.

Because the 65-Series cascade data (Ref. 7) were obtained with inlet air angle fixed, the $(d\delta/di)_{ref}$ obtained from Lieblein's curves is applicable to a constant inlet air angle cascade, while, as Smith (Ref. 11) pointed out, in practical applications the blade stagger angle, γ, is fixed and the inlet air angle varies. Smith (Ref. 11) developed relations to obtain $(d\delta/di)_{ref}$ applicable to fixed-γ blade rows from Lieblein's correlations and gave a numerical example in which the fixed-γ derivative was larger than the fixed-β_1 derivative by a factor of three for NACA 65-(12) 10 blades with $\sigma = 1$ and $\beta_1 = 60$ degrees. Figure 8 shows the variation of deviation angle with incidence angle from Reference 7 for the NACA 65-(12) 10 blades (see Ref. 12 for blade nomenclature) of Smith's (Ref. 11) example at a constant inlet air angle, $\beta_1 = 60$ degrees. Data of Reference 7 were crossplotted to obtain a second curve shown in Figure 8 for the same blades with a constant stagger angle of 47.6 degrees which is the stagger angle of a cascade of NACA 65-(12) 10 blades

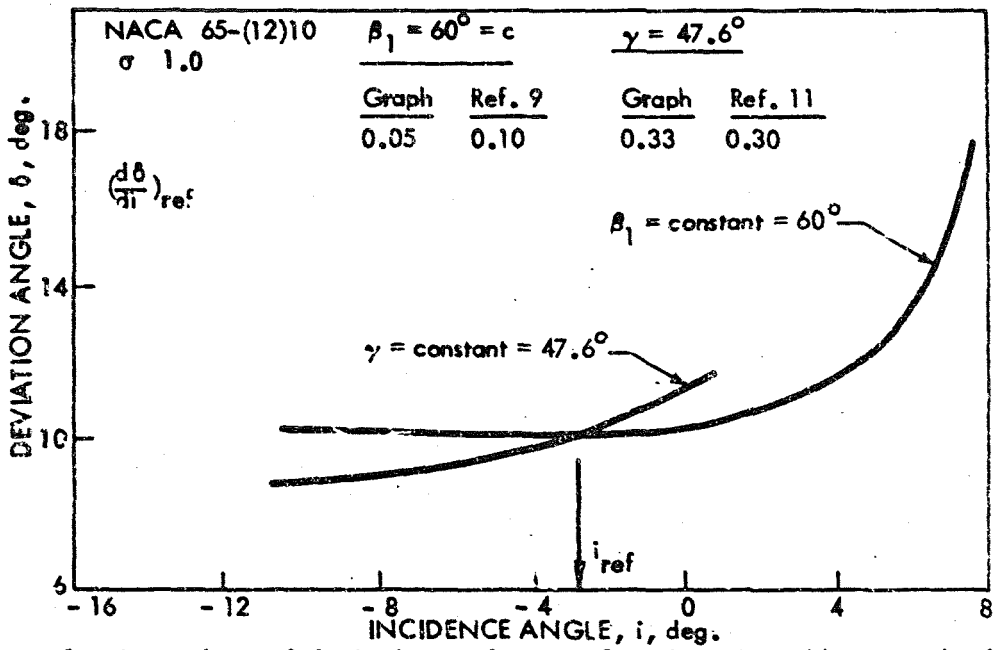

Figure 8 — Comparison of deviation angle as a function of incidence angle for constant inlet angle and constant stagger angle. Data from Reference 7.

with β_1 = 60 degrees, σ = 1.0, and $i = i_{ref}$ where i_{ref} was computed using the correlations of Reference 9. Graphically determined values of $(d\delta/di)_{ref}$ are compared with values from Lieblein's (Ref. 9) correlation and Smith's (Ref. 11) calculation. Based on the differences in this example it appears that the fixed-γ derivative should be used in preference to fixed-β_1 derivatives in analysis applications when computing the change of deviation angle for a change of incidence angle in the low-loss incidence angle interval. Smith (Ref. 11) also pointed out that the fixed-γ derivative was strongly dependent on camber and therefore the fixed-β_1 derivative should be also.

Howell (Ref. 13) presented a single curve for $(\delta - \delta_{nom})/\epsilon_{nom}$ as a function of $(i - i_{nom})/\epsilon_{nom}$ where the nominal conditions occur at 0.8 of the turning angle at which the loss is twice the minimum value.

Apparently no method (empirical or analytical) has been published as yet to predict the functional relation between deviation angle and incidence angle

outside the low-loss incidence angle interval even for a plane two-dimensional caacade flow. It seems highly probable that the blade surface boundary layers play a decisive role in determining the deviation angle outside the low-loss region and therefore boundary layer considerations would strongly enter into any successful correlation or analytical method which might be devised.

Annular Cascades

No correlations are available which express the relationship between deviation angle and incidence angle specifically for annular cascades. The alternative is to apply the plane cascade methods to annular cascades, although because of the complicated three-dimensional flow in the latter the deviation angle is sometimes observed to decrease as incidence angle increases (e.g. Ref. 14) rather than increase as in plane cascades.

In these first two sections, methods of predicting deviation angle were reviewed which assumed that the stream surfaces are surfaces of revolution and that the flow around a given blade section is not influenced by the flow around adjacent blade sections. In some blade rows the flow deviates sufficiently from this two-dimensional model that corrections accounting for the three-dimensionality of the flow must be applied to the two-dimensional deviation angles. These corrections are usually obtained by considering the predicted axisymmetric exit flow field (obtained using two-dimensional δ) rather than attempting to define further geometric parameters. The sections which follow review a number of attempts to incorporate the effects of three-dimensional flow into deviation angle prediction methods.

AXIAL VELOCITY RATIO

It is well known that the deviation angle in a rectilinear or plane cascade depends on the ratio of the leaving to the entering axial velocities (AVR). Katzoff, et al. (Ref. 15) among others reported the phenomenon in 1947. Because of this effect, discrepancies exist between deviation angle data measured under two-dimensional conditions in cascades with side and end wall suction and data measured in similar cascades with solid walls. The leaving axial velocity in a solid wall cascade is usually higher because of the general increase of boundary layer thickness and particularly because of regions of separation in the corner where the blade suction surface intersects the side wall. These regions of separation reduce the effective flow area which raises the general level of axial velocity leaving the blade row. Elimination of these regions of separation and establishment of a constant axial velocity through the cascade can be accomplished by continuous boundary-layer removal through porous walls as described in Erwin and Emery (Ref. 16). A constant axial velocity is a consequence of continuity for the two-dimensional flow of an incompressible fluid.

The changes in flow through a cascade as axial velocity ratio changes may be described by considering the accompanying change in pressure distribution. If the losses are assumed constant for a small change in AVR then the static pressure rise across a blade in a cascade decreases (increases) as AVR increases (decreases) assuming incompressible flow. The resulting change in pressure distribution is illustrated in Figure 9. In general the airfoil circulation may also be expected to change as AVR varies. The magnitude of the change in circulation has a direct effect on the change in deviation angle. Evaluating circulation using the path EFGH of Figure 10, assuming

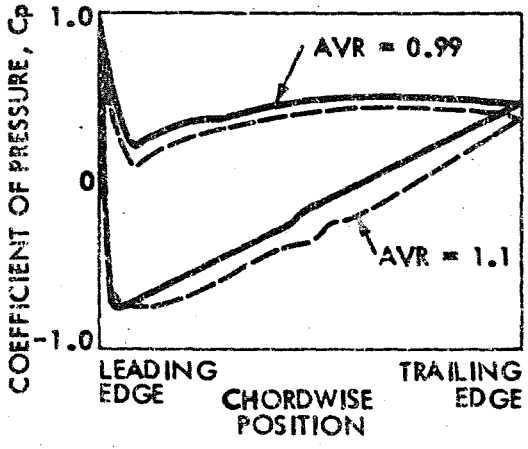

Figure 9 – Effect of axial velocity ratio on cascade blade pressure distribution (Ref. 17).

$s_1 = s_2$, yields the result

$$\Gamma = s(V_{\theta,1} - V_{\theta,2}). \qquad (5)$$

From the velocity diagrams in Figure 10 it is apparent that the deviation angle will decrease as AVR increases if circulation increases (i.e. $V_{\theta,2}$ decreases) or unless the circulation decreases enough so that $V_{\theta,2}$ increases by more than d units. Similarly if circulation decreases (or increases less than a critical amount) deviation angle will increase as AVR decreases. In fact available experimental results (Refs. 15 – 18) indicate that deviation angle does decrease with increasing AVR and increases with decreasing AVR,

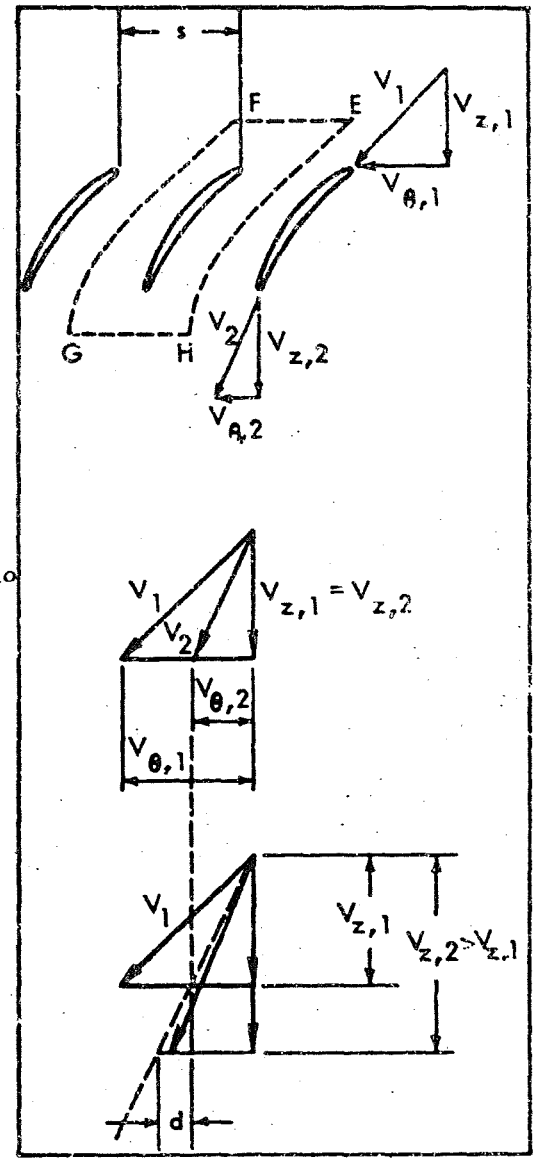

Figure 10 – Effect of axial velocity ratio on plane cascade velocity diagrams.

although the data of Reference 16 indicate that circulation decreases slightly as AVR increases.

Plane Cascades

Empirical Methods

Pollard and Gostelow (Ref. 17) and Montgomery (Ref. 18) have presented experimental results which indicate deviation angle is a linear function of axial velocity ratio over a limited interval. Pollard and Gostelow's (Ref. 17) data were obtained in a porous wall tunnel by varying the amount of wall suction to control axial velocity ratio. A cascade with 10C430C50 blade sections (see Ref. 5 for blade nomenclature) was tested at solidities of 1.0 and 1.14. Stagger angle was 36 degrees and the nominal inlet air angle was 52 degrees 50 minutes. Deviation angles measured for the interval $0.93 \leq AVR \leq 1.1$ can be approximated by the equation

$$\delta = \delta_{AVR=1} - 10(AVR - 1) \tag{6}$$

where $\delta_{AVR=1}$ is the deviation angle for AVR = 1. For a solidity of 1, $\delta_{AVR=1} = 9.5$ degrees.

Montgomery (Refs. 18 and 19) obtained his data in a solid wall tunnel using a 9-blade cascade with an aspect ratio of 4.1. The blades had a NACA 65-410 profile, (equivalent circular arc camber = 10 degrees), 4.875-inch chord, 20-inch span, and a solidity of 1. The inlet flow angle was varied from 48 to 62 degrees. Turning angle data at various axial velocity ratios were obtained by operating the tunnel in three configurations. The first configuration consisted of exhausting to atmosphere in a convention manner. The second configuration featured a 4-inch diameter cylinder placed at midspan with its centerline 6 inches downstream of the trailing edge of the

cascade. The third configuration consisted of the cascade with an 8-inch. channel shaped, screen placed 4 inches downstream of the cascade trailing edge. The obstructions downstream reduced the outlet axial velocity (hence AVR) by varying amounts over the midspan portion of the cascade, with the maximum reduction at midspan. A further variation of AVR was obtained by varying the inlet air angle (hence incidence angle).

Two series of tests are reported by Montgomery (Ref. 18), the first being measurements at midspan for various inlet air angles with no obstruction and with the screen obstruction downstream. The second series of tests were made at an inlet air angle near stall with the circular cylinder and the screen obstacles downstream. Measurements of flow angles and velocities were obtained at several spanwise positions from midspan to one end of the blade. The difference between measured and two-dimensional (Ref. 7) deviation angles was plotted versus axial velocity ratio in Reference 18 for all data in both series of tests and can be reasonably approximated by

$$\delta = \delta_{AVR=1} - 12\ (AVR - 1). \tag{7}$$

Extreme caution should be exercised in the interpretation or use of Montgomery's (Ref. 18) results however, because of the three-dimensional flows which existed in his cascade flow field.

Part of the results of the much more extensive investigation of Heilmann (Ref. 20) is reported by Heilmann, et al. (Ref. 21) and is reproduced as Figure 11. The change of turning angle (the negative of the change in deviation angle) is shown as a function of inlet angle for a NACA T1-$(18A_6I_{4b})$08 cascade (see Ref. 22 for blade nomenclature). The angle of attack was held constant by restaggering the cascade for each value of β_1. The band represents the range of values of the slope of the turning angle versus axial velocity

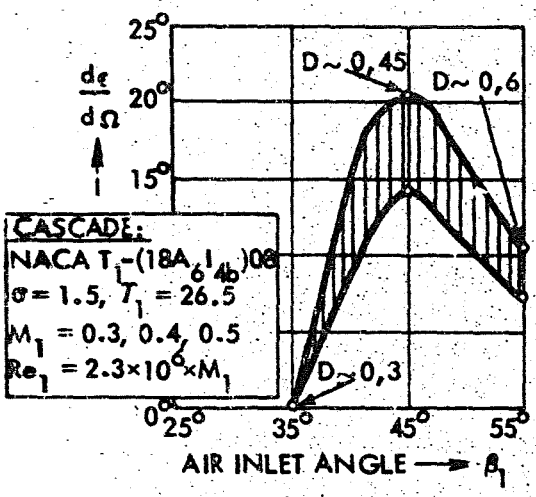

Figure 11 — Derivative of fluid turning angle with respect to axial velocity density ratio for various air inlet angles (Ref. 21).

angle at plane b, β_{cor}, was assumed to be the angle which would be measured at the outlet with no flow contraction (i.e. two-dimensional flow). A further change in flow angle which occurs between plane b and the exit plane, 2, due to contraction of the flow was calculated by applying the momentum theorem to a control surface between plane b and plane 2 (Fig. 12). The following relationship was obtained,

density ratio, Ω, curve and therefore indicates that a nonlinear variation of deviation angle and axial velocity density ratio was obtained. This curve also indicates that corrections using Equations (6) and (7) have questionable validity because of the limited data on which they are based.

Semi-Empirical Methods

Scholz (Ref. 23) considered a simplified flow model in which the blade turning action was concentrated at a plane b located inside the blade row (see Fig. 12). The flow

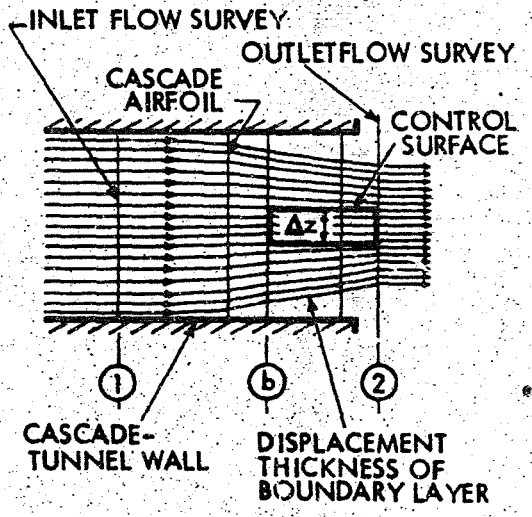

Figure 12 — Flow in a plane, solid wall cascade after Reference 23.

$$\tan \alpha_{2cor} = (Q_2/Q_b)\tan \alpha_2 \qquad (8)$$

where Q_b and Q_2 are the mass rate of flow at planes b and 2 per unit of width and for one spacing of the cascade. Scholz (Ref. 23) asserts that Q_b may be related to Q_1 by

$$\frac{Q_b - Q_1}{Q_2 - Q_1} = \text{constant} = k(b) \qquad 0 < k(b) < 1 \qquad (9)$$

where k is to be experimentally determined.

Erwin and Emery (Ref. 16) presented three methods of correcting for the axial velocity increase in a solid wall cascade. The first method computes the corrected turning from an exit velocity diagram which has axial velocity equal to the entrance axial velocity and tangential velocity equal to the measured value (Fig. 13a). The inlet velocity diagram is assumed unchanged. In the second method the inlet diagram is unchanged, but the outlet axial velocity is corrected to the mean of the inlet and outlet values (Fig. 13b). Outlet tangential velocity is assumed constant. The third method adjusts both inlet and outlet axial velocities. The inlet axial velocity is taken to be less than the mean axial velocity by one-half the axial velocity increase due to the blockage effect of the wake. The corrected outlet axial velocity is greater than the mean axial velocity by one-half the wake increment (Fig. 13c). All three methods assume tangential velocities, and hence circulation, remain unchanged. All these corrections were applied to solid wall cascade data presented in Reference 16. The data were obtained for NACA 65-(12)10 (equivalent circular arc camber = 30.2 degrees) profiles at inlet air angle of 60 degrees, solidity of 1, and aspect ratio of 4. Data were also obtained in a porous wall cascade for an aspect ratio of 1 and 2. Incidence angle was varied by restaggering the cascade over the interval

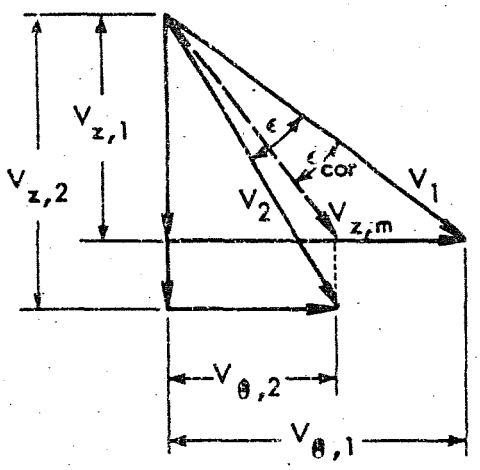

(a) Outlet axial velocity corrected to inlet axial velocity.

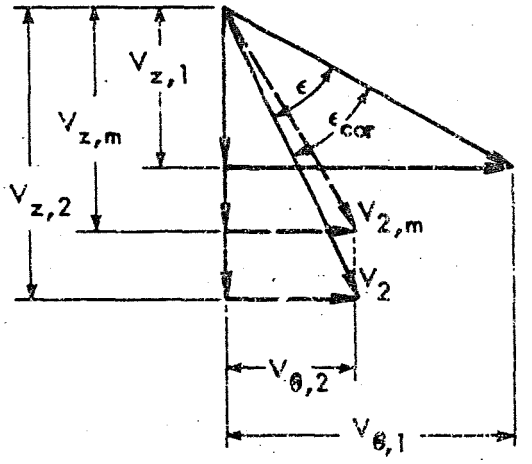

(b) Outlet axial velocity corrected to mean axial velocity.

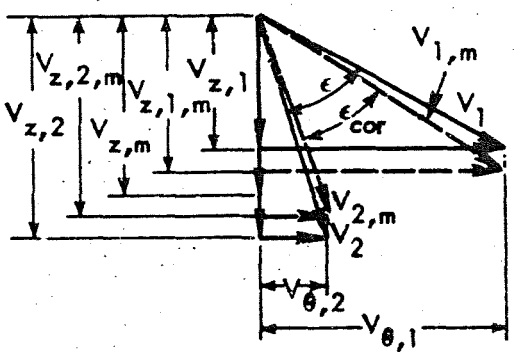

(c) Outlet and inlet velocities corrected to mean values.

Figure 13 – Axial velocity ratio corrections of Reference 16.

from 39 to 50 degrees. The deviation angles measured in the solid wall cascade were 2 to 4 degrees less than those from the porous wall cascade in which the flow was two-dimensional. The second and third methods reduced the discrepancy by about one-half (under correction). The first method tended overcorrect, but the resulting corrected deviation angles were within 1 degree of the two dimensional values.

Potential Flow Methods

The effects of changing axial velocity through a plane cascade have been calculated using the method of singularities by Pollard and Horlock (Ref. 24), by Mani and Acosta (Ref. 25), and by Shaalan and Horlock (Ref. 26).

Kubota (Ref. 27) has made a similar calculation using conformal transformations.

Pollard and Horlock (Ref. 24) extended the method of singularities as presented in Reference 28 for computing cascade performance. The method of singularities as applied by Pollard and Horlock (Ref. 24) basically consists of superimposing a uniform flow and the flow from a distribution of sources, sinks, and vortices on the chord lines of an infinite cascade. The source and vortex strength distributions are selected so that each blade surface of the cascade coincides with a streamline, the velocity normal to the mean camber lines is zero, and the vorticity is zero at the trailing edges (Kutta-Joukowski condition). Since the net outflow of the sources and sinks is required to be zero, no change in axial velocity through the cascade occurs.

However, in the extended method of Pollard and Horlock (Ref. 24), infinitely long strip sources and sinks, extending in the tangential direction, were added to the flow field between the leading and trailing edge planes of the cascade (Fig. 14). The combined flow was again required to have a streamline identical with each blade of the cascade and to satisfy the Kutta-Joukowski condition at the trailing edge. The number of strip singularities per unit length in the axial direction was constant as was the strength per unit length in the tangential direction. This uniform distribution of source strength produced a linear variation of axial velocity through the cascade. Half the flow from the strip sources flows upstream and half downstream

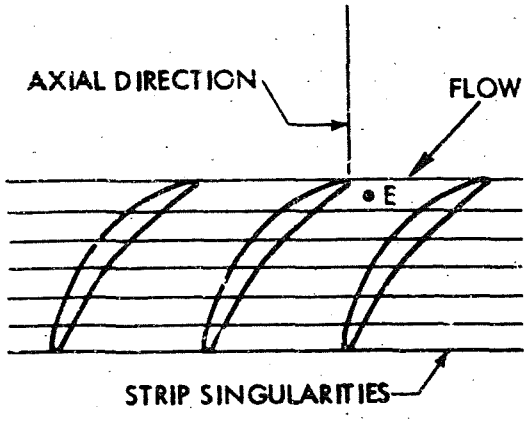

Figure 14 — Distribution of strip singularities.

leaving the axial velocity unchanged at the mid-chord position, but adding to the flow field at each point E, Figure 14, an axial component of velocity proportional to the source flow between the point E and the mid-chord position. Since the source strength was uniform in the axial direction a linear variation of velocity within the cascade resulted. By computing the total circulation on a blade with and without the strip sources the change in deviation angle for various axial velocity ratios was computed.

Results were given for a cascade of 10C430C50 profile blades with a stagger angle of 36 degrees. Solidity was 1 and the incidence angle was 1.8 degrees. The calculated results are shown in Figure 15. The change in deviation angle for the axial velocities shown can be approximated within 0.1 degree by the linear equation

$$\delta = \delta_{AVR=1.0} - 7.67\ (AVR - 1.0). \quad (10)$$

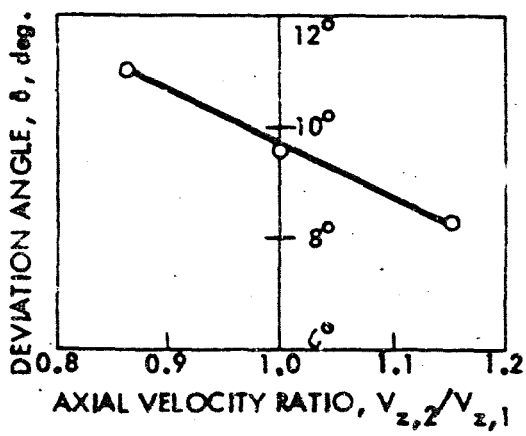

Figure 15 — Calculated variation of deviation angle with AVR for a cascade of 10C430C50 profiles at 36 degree stagger (Ref. 24).

Note that Equation (10) differs from Equation (6) which was obtained experimentally by Pollard and Gostelow (Ref. 17) although the deviation angle calculated at AVR = 1 by Pollard and Horlock is very close to the experimental values. Whether the difference between Equations (6) and (10) is due to an error in the analysis, in the experimental data, or in both is not apparent.

In a later paper Shaalan and Horlock (Ref. 26) present a different approach which also employs the method of singularities. In this approach

the continuity equation was reduced by an approximation into a Poisson partial differential equation for the velocity potential

$$\frac{\partial^2 \phi}{\partial x^2} + \frac{\partial^2 \phi}{\partial y^2} = f(x, y) = -\frac{1}{x}\left(\frac{\partial \phi}{\partial x}\right) \tag{11}$$

This equation was solved by an iterative process. First, the incompressible, two-dimensional solution was obtained (i.e. $\partial^2\phi/\partial x^2 + \partial^2\phi/\partial y^2 = 0$) and then $f(x, y)$ was evaluated from this approximation. Plane sources were then located in the blade passage with strength equal to $f(x, y)$. Velocities induced at the blade surface by these plane sources were computed and canceled by a line of sources and sinks at the profile. From this combination of velocity potentials a new evaluation of $f(x, y)$ is obtained and used to distribute more plane sources, etc. until convergence is reached. The circulation and exit flow angle can be computed from the final singularity distribution and the basic uniform flow. The mean axial velocity varies linearly through the cascade. It was also assumed in the solution that axial velocity varied linearly from the suction surface of one blade to the pressure surface of the next blade.

Pressure distributions and turning angles were computed for the same 10C430C50 cascade mentioned above. The deviation angle calculated for AVR = 1 was 8 degrees and for AVR = 1.10, δ = 7.5 degrees. Thus both the magnitude and the change in deviation angle calculated with this method seem to be less than those measured by Pollard and Gostelow (Ref. 17) for the same cascade. A possible explanation of this discrepancy may lie in the fact that the results of Shaalan and Horlock (Ref. 26) were obtained from only one iteration of the solution method.

Kubota (Ref. 27) has presented a method of predicting the effect of axial velocity changes on cascade turning in which sources (or sinks) were uniformly

distributed in the blade passages to produce a linear variation of axial velocity through the blade row. He considered three elementary flows: 1) The cascade flow with no change in axial velocity; 2) Flow from the source (or sink) distribution which provided the desired axial velocity change, but did not satisfy the boundary condition of zero normal velocity at the blade surface (applied at a corresponding point along the chord as in thin airfoil theory); and 3) Flow from additional sources, sinks, and vortices distributed on the chord line to satisfy the boundary condition and the Kutta-Joukowski condition at the trailing edge.

To determine the third elementary flow, the blade was mapped onto a unit circle. A relation was thus obtained to compute the difference in circulation between the first elementary flow and the superposition of the three elementary flows. This difference in circulation then represents the circulation change due to the change in axial velocity. Kubota presented curves which allow this change in circulation to be computed for cascades of zero-thickness flat plates and for NACA 65-series compressor cascades. He then divided the corresponding change in circumferential velocity equally between the inlet and outlet flow to obtain the deviation angle for axial velocity ratios other than one.

Mani and Acosta (Ref. 25) considered flow through an infinite plane cascade in which the distance between stream surfaces is a slowly varying function of axial distance. They averaged the continuity equation across the stream tube to obtain a Poisson equation for the average velocity potential

$$\frac{\partial^2 \hat{\Phi}}{\partial x^2} + \frac{\partial^2 \hat{\Phi}}{\partial y^2} = \frac{(dh/dz)}{h} \frac{\partial \hat{\Phi}}{\partial x} \tag{12.}$$

where h is the streamtube height. The method of solution was modeled on that of Mellor (Ref. 29) and consisted of distributing sources and vortices on the

blade chord line which, when superimposed on a uniform flow, result in a flow approximately tangential to the blade surface. The singularities used were required to satisfy the Poisson Equation (12) rather than the Laplace equation. Stream surface or channel shapes were restricted to those with constant height both upstream and downstream of a segment with exponentially decreasing height. The cascade was located arbitrarily with respect to the converging section. Deviation angle results were presented for a circular arc cascade having $C_{\ell o}$ = 1.00 (camber = 25 degrees), stagger angle = 45 degrees, an axial velocity ratio of 1.13 and 1.0, and solidities ranging from 0.5 to 1.15. At an angle of attack of 15 degrees (incidence angle 2.5 degrees) the computed deviation angle for AVR = 1.13 was larger than the deviation angle at AVR = 1.13 for all solidities and was, for example, about 1.3 degrees larger at a solidity of 1.00. This result does not seem to be consistant with measurements from similar cascades such as that of Reference 17. At zero angle of attack (incidence angle = - 12.5 degrees), the deviation angles for AVR = 1.13 were smaller than those for AVR = 1.0 for all solidities except the solidity of 1.25, where they were approximately the same. The results are not presented in a readily usable form, however a computer program is available (Ref. 30).

Annular Cascades

Axial velocity changes across annular cascades result from annulus boundary layer growth and corner stall effects as in plane cascades. However additional and perhaps dominant causes for annular cascades are noncylindrical hub and casing contours, radially varying energy transfer and pressure losses, and curvature which because of radial equilibrium and continuity requirements usually result in a change of axial velocity from inlet to outlet along a stream surface.

When two-dimensional cascade data are applied in the design or analysis of annular cascades it must be corrected to reflect the effect of the annular cascade axial velocity ratio. If it is assumed that the change in deviation angle from the two-dimensional value depends only on the value of the axial velocity ratio and not on the manner in which it arises, then the plane cascade corrections from the previous section may be applied.

For example, Schulze, et al. (Ref. 31) used a two-dimensional method to correct data from a compressor rotor for comparison with two-dimensional cascade data. In the rotor test axial velocity ratio was varied by atteching fairings to the rotor hub thereby changing the annulus area. Measured rotor turning angles for three blade sections were given for exit to entrance annulus area ratios of 1.15, 1.0, 0.85 and 0.70. These rotor turning angles were corrected back to "two-dimensional" values using two methods. In the first method (see Fig. 13a), circulation was assumed constant and the equivalent exit axial velocity was taken to be equal to the inlet axial velocity. This method substantially overcorrected the rotor data as compared with two-dimensional cascade data. The second method (see Fig. 13b), also assumed constant circulation, but adjusted both the entrance and exit axial velocities to a mean value. This method was more satisfactory, but also tended to over-correct.

The mean axial velocity method was also used to correct two-dimensional cascade data for comparison with the measured rotor data taken near design angle of attack. The comparisons for A_2/A_1 of 0.85 were quite good, however they were less favorable for A_2/A_1 of 1.15, 1.0, and 0.70. The limitations of the method were acknowledged (Ref. 31) and recommended application was limited to axial velocity changes of 15 percent or less. Essentially the same method is given by Jansen and Moffatt (Ref. 32).

SECONDARY FLOW

Secondary flow in turbomachines has been defined in several ways. Herzig, et al. (Ref. 33) define secondary flows as "any motion of boundary-layer fluid having components of motion normal to the through-flow directions." Louis (Ref. 34) and Rohlik, et al. (Ref. 35) give similar definitions terming secondary flow the deviation in boundary-layer flow from the free stream or main stream flow direction. Smith (Ref. 36) defines secondary flow as the difference between the actual flow and the "primary flow," where the "primary flow" is that flow obtained from successive application of the axisymmetric and blade-to-blade methods assuming the flow to be frictionless. Smith's definition includes as secondary flow any nonboundary-layer flow which is normal to the axisymmetric stream surfaces of revolution in addition to all boundary-layer flow. Because the "primary flow" is well defined it is possible to express the secondary flow quantitatively. Using Smith's definition, Lakshminarayana and Horlock (Ref. 37) have listed the following secondary flows:

1. Cascade secondary flow
2. Mainstream secondary flow
3. Tip clearance leakage flow
4. Scraping vortices
5. Radial flows of the blade surface boundary layers.

A complete review of the large amount of literature treating various aspects of secondary flow was considered impractical, therefore only selected, representative work which is applicable to the prediction of deviation angles in turbomachinery will be reviewed in this section. No discussion will be given concerning items 4 and 5 of the above list because of an apparent lack of quantitative methods of deviation angle prediction.

Cascade Secondary Flow

Cascade secondary flow occurs when a flow with annulus wall boundary layers is turned in a blade row. It is simply the cross-flow component of the skewed annulus boundary layers which form in the blade passage together with the resulting circulatory flow set up in the surrounding fluid.

Within the blade passage a blade-to-blade static pressure gradient exists in the free stream flow outside the boundary layer. This static pressure gradient, caused by the curvature of the streamlines in the blade-to-blade plane, is principally determined at any point by the local radius of curvature of the streamline, R_c, and by the magnitude of velocity. The relationship is approximately given by

$$\frac{dp}{d\zeta} = \frac{V^2}{g_c R_c} . \tag{13}$$

If the boundary layer is thin, the freestream static pressure gradient may be assumed to be impressed upon the boundary layer which because of its lower velocity must then have streamlines with a smaller radius of curvature (see Eq. (13), giving rise to a crossflow component as illustrated in Figure 16.

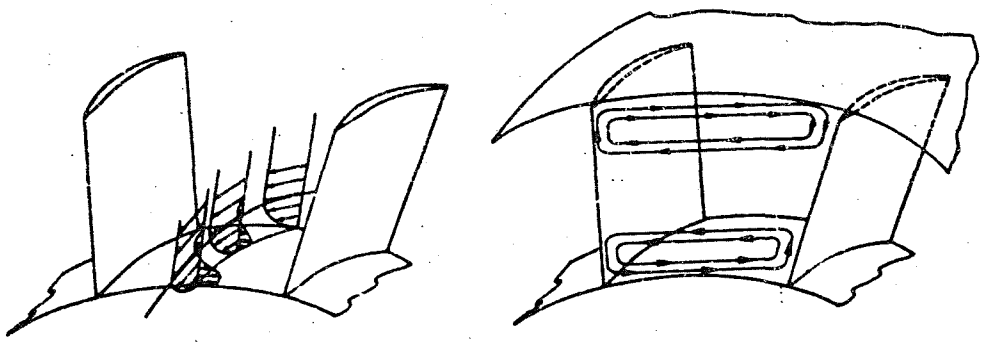

(a) Annulus boundary layer velocity components.

(b) Circulatory representation of cascade secondary flow.

Figure 16 — Cascade secondary flow.

The cross-flow results in an overturning of the boundary layer fluid (decreased deviation angle) as compared to the free stream fluid. Underturning is usually observed near the edge of the boundary layer (e.g. Ref. 34) suggesting that a small cross-flow component exists in the opposite direction and extends a short distance into the free stream as indicated in Figure 16a. The resulting secondary flow pattern is sometimes represented as shown in Figure 16b.

In a real blade row it is necessary to be able to predict the under- or over-turning as compared to the turning which is predicted from two-dimensional cascade results. Because exact solutions to turbulent, three dimensional boundary layer problems are not attainable at present, theoretical attempts to predict cascade secondary flow turning have been based on approximations to the real flow. Usually the flow is assumed to be inviscid and incompressible, but not irrotational, that is vorticity components due to previous viscous action are allowed. The entering flow in Figure 16 for example has a vorticity component normal to the streamwise direction in the boundary layer. At the outlet, as a result of the turning imposed on the main stream, a vorticity component in the streamwise direction also appears in the regions where over- or under-turning occurred. If the streamwise vorticity component is known, then for inviscid, incompressible flow the corresponding secondary (or cross-flow) velocities may be found from which the over- and under-turning may be determined. Hawthorne (Ref. 38) derived an expression for the change in the streamwise vorticity component for inviscid, incompressible flow in a curved channel, Figure 17. His equation is

$$(\zeta/V)_2 - (\xi/V)_1 = -2\int_{\epsilon_1}^{\epsilon_2} \frac{\nabla P}{\rho}\frac{1}{V^2}\sin\eta\, d\epsilon \qquad (14)$$

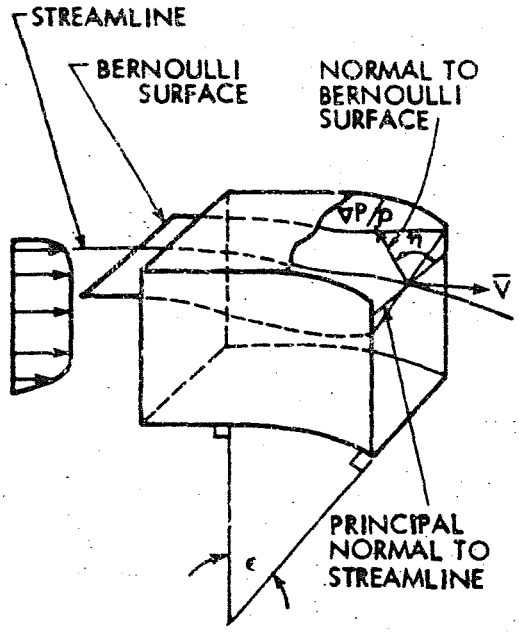

Figure 17 – Inviscid, rotational flow through a curved duct.

where

P = stagnation pressure

ξ = streamwise vorticity

ε = angle of turning of the fluid

η = angle between the normal to the Bernoulli surfaces and the principal normal to the streamline

V = fluid velocity

ρ = fluid density.

A Bernoulli surface is composed of intersecting vortex lines and streamlines and is a surface of constant stagnation pressure in a steady, inviscid flow. Starting with Equation (14) and assuming the inlet streamwise vorticity component to be zero and that the stagnation pressure varies only in the spanwise direction, Lakshminarayana and Horlock (Ref. 39) have presented a solution for the cascade secondary velocities at the outlet of a stationary cascade which is valid for small turning angles. Their solution includes the effect of Bernoulli surface rotation and viscous diffusion of the velocity profile from the inlet station to the trailing edge of the cascade. Accounting for the latter effect tailors the solution for an idealized experimental situation where an annulus boundary layer profile is simulated at the midspan of the cascade by a wake created artificially upstream of the cascade (Fig. 18). Applicability of this part of the analysis to annulus wall boundary layer regions depends on the similarity of viscous diffusion at the edges of wakes

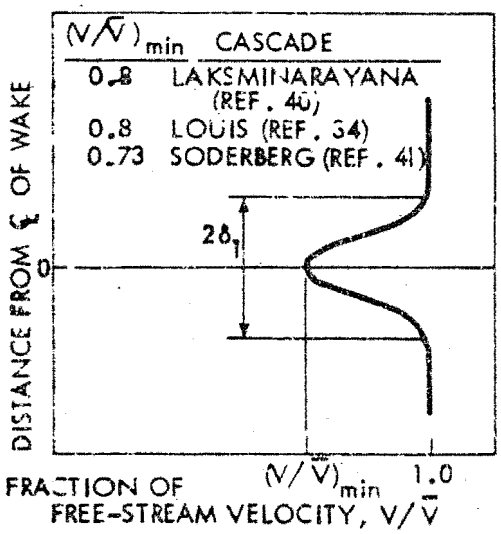

Figure 18 – Central wake profile.

and boundary layers. A secondary stream function is defined such that

$$u_s = \frac{\partial \psi_s}{\partial y}, \quad w_s = -\frac{\partial \psi_s}{\partial x} \tag{15}$$

and

$$\nabla^2 \psi_s = -\xi_2 \quad 0 < y < \delta_1 \tag{16}$$

$$\nabla^2 \psi_s = 0 \quad \delta_1 < y. \tag{17}$$

Rather lengthy expressions (not reproduced here) are given in Reference 39 for ψ_s and for the change in angle from the free-stream angle as a function of $\partial\psi_s/\partial y$. Numerical methods using a digital computer would usually be necessary to obtain a quantitative solution. Theoretically calculated turning angles are compared in Reference 39 with the experimental results of Lakshminarayana and Horlock (Ref. 40), Soderberg (Ref. 41) and Louis (Ref. 34). The three sets of experimental results were obtained from cascades with central wakes, Figure 18, simulating an inlet boundary layer profile. Detailed information on the three cascades is given below.

	Lakshminarayana's (Ref. 40) cascade	Soderberg's (Ref. 41) cascade	Louis' (Ref. 34) Cascade
Profile description	10C430C50	NACA 6409	10C430C50
Camber, deg.	30	28	30
Blade chord, in.	6	4.5	6
Aspect ratio	4.83	3.56	3.0
Solidity	1.00	1.01	1.00
Blade setting angle, deg.	36	30	36
Incidence angle, deg.	1	15	4
Blade chord Reynolds number	2×10^5	2.8×10^5	2.5×10^5

The theoretical results compared very closely with experimental values with only a few exceptions and even these discrepancies were 1 degree or less. Some question remains however regarding accuracy of the procedure near a wall which is the real configuration of interest. For example, Louis (Ref. 34) also gives turning angle data for a cascade identical to Lakshminarayana's except that a thin wall was installed between the blades at midspan dividing the inlet wake flow, a configuration which more nearly approximates annulus wall flow. Very much larger overturning was measured for this configuration which had a region of separated flow near the corner formed by the suction surface of the blade and the wall, indicating that the analysis would not give correct predictions when corner stall is present. An evaluation of the method using data near a wall in the absence of corner stall apparently has not been made.

Mainstream Secondary Flow

A key assumption necessary to obtain an axisymmetric solution is that the stream surfaces are surfaces of revolution or axisymmetric stream surfaces as shown in Figure 19.

Any flow perpendicular to the axisymmetric stream surface is defined as secondary flow. It is very unlikely that stream surfaces in any real annular cascade are surfaces of revolution. Vavra (Ref. 42) has discussed at some length the requirements for the existence of axisymmetric stream surfaces in both stationary and rotating cascades for steady, isentropic (irrotational for stators) flow and has concluded it is unlikely that blades can be designed to produce axisymmetric stream surfaces even for this idealized flow. Real stream surfaces are warped as illustrated in Figure 19 with the direction and magnitude of the warping dependent on the blade geometry.

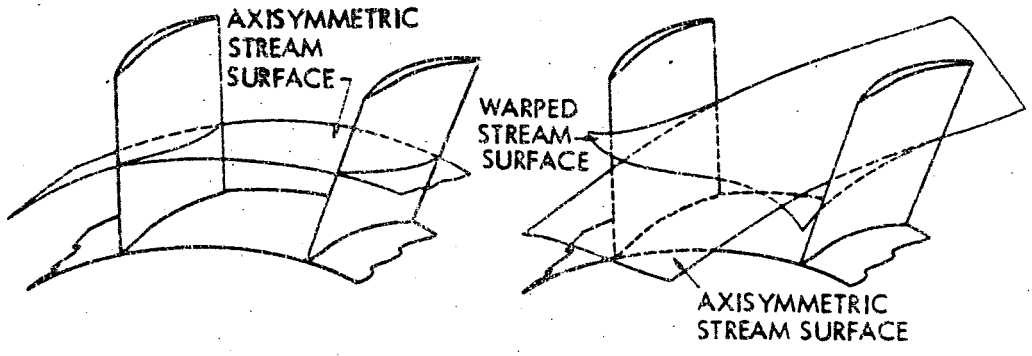

Figure 19 — Axisymmetric and warped stream surfaces.

Some insight into the reasons the stream surfaces are warped may be gained by considering a simple example: irrotational, incompressible flow through a stationary, free-vortex blade row with cylindrical annulus walls. One blade passage is represented in Figure 19. The governing equations for the flow in cylindrical coordinates are the irrotationality condition,

$$\nabla \times \vec{V} = \hat{r}\,\frac{1}{r}\left(\frac{\partial V_z}{\partial \theta} - \frac{\partial (rV_\theta)}{\partial z}\right) - \hat{\theta}\,\frac{1}{r}\left(\frac{\partial V_z}{\partial r} - \frac{\partial V_r}{\partial z}\right) + \hat{z}\left(\frac{\partial (rV_\theta)}{\partial r} - \frac{\partial V_r}{\partial \theta}\right) = \vec{0} \qquad (18)$$

and the continuity equation,

$$\frac{1}{r}\frac{\partial (rV_r)}{\partial r} + \frac{1}{r}\frac{\partial V_\theta}{\partial \theta} + \frac{\partial V_z}{\partial z} = 0. \qquad (19)$$

Each term of Equation (18) is equal to zero giving,

$$\frac{\partial V_z}{\partial \theta} = \frac{\partial (rV_\theta)}{\partial z} \qquad (20)$$

$$\frac{\partial V_z}{\partial r} = \frac{\partial V_r}{\partial z} \tag{21}$$

$$\frac{\partial (rV_\theta)}{\partial r} = \frac{\partial V_r}{\partial \theta} . \tag{22}$$

Upstream of the cascade all derivatives with respect to θ are zero because of the symmetry of the flow. Thus by Equation (20) two flow configurations are possible, either rV_θ is a constant or V_θ is zero. In a cylindrical annulus derivatives with respect to z will also vanish in the flow upstream of the cascade and thus by Equation (21).

$$\frac{\partial V_z}{\partial r} = 0 \tag{23}$$

indicating the stream surfaces are cylindrical as would be expected. Because the cascade is composed of free-vortex blading the circumferential average value of rV_θ is assumed to be constant downstream of the cascade although circumferential gradients of velocity exist. In a real, viscous flow mixing would occur so that axisymmetric flow would be approached at some distance downstream from the cascade. If the efficiency of the mixing was constant and not a function of radius, then after the mixing rV_θ would be constant throughout the flow and cylindrical stream surfaces would exist. Perhaps because of this it is often assumed that axisymmetric stream surfaces exist in the blade passages of free-vortex cascades. For this to be true, it would be necessary that

$$\frac{\partial V_r}{\partial \theta} = 0 \tag{24}$$

inside the blade passage. From Equation (21) this is true only if

$$\frac{\partial (rV_\theta)}{\partial r} = 0. \tag{25}$$

Vavra (Ref. 42) shows that it is not possible to design a stationary cascade with an infinite number of blades which will satisfy Equation (25) and concludes that it is also unlikely that a cascade with a finite number of blades could satisfy it. It is, however, difficult to speculate on the directions of secondary flow in a free-vortex cascade. For a free-vortex cascade with irrotational flow it is assumed that

$$r_2 \bar{V}_{\theta,2} = \text{constant} \tag{26}$$

and the circulation of a blade element

$$\Gamma = s(V_{\theta,1} - \bar{V}_{\theta,2}) \tag{27}$$

$$= \frac{2\pi r}{n} (V_{\theta,1} - \bar{V}_{\theta,2}) = \text{constant} \tag{28}$$

because the product rV_θ is constant both upstream and downstream of the blades. Thus circulation is constant along the span of the free-vortex cascade.

The circulation will increase along the span of a stationary cascade if for example,

$$rV_{\theta,1} = \text{constant} \tag{29}$$

and

$$\bar{V}_{\theta,2} = \text{constant} < 0. \tag{30}$$

Such a cascade is represented in Figure 20. Along a line of constant radius EF the change in V_r is determined by Equation (22). If rV_θ is on the average a strongly increasing function of r then it seems reasonable that at most or all points of EF

$$\frac{\partial V_r}{\partial \theta} > 0. \tag{31}$$

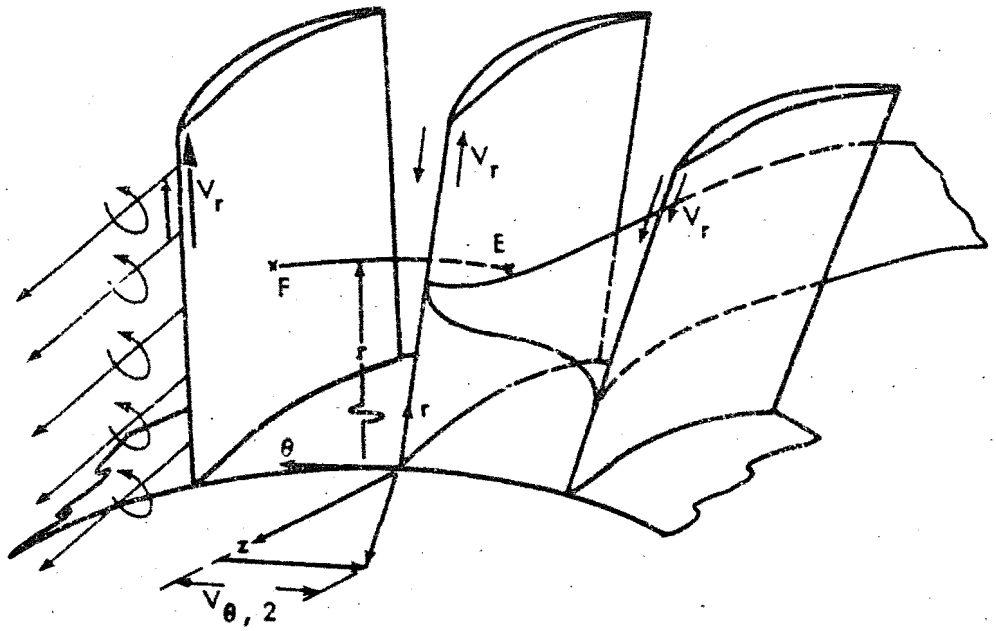

Figure 20 – Main stream secondary flow.

Thus the radial velocity is larger on the pressure surface than on the suction surface. Three possible relationships between the radial velocity on the pressure and suction surface are illustrated at the trailing edges of the blades in Figure 20. Regardless of the absolute level of magnitude of V_r, the stream surface will at least qualitatively resemble the surface shown in Figure 20, and velocities normal to the stream surfaces of the axisymmetric solution will exist and are defined as main-stream secondary flow caused by a spanwise gradient of circulation. This discontinuity in radial velocity is often represented by a sheet of vortices extending downstream from the trailing edges of the blades. This flow field tends to cause underturning toward the tip of the blade and overturning toward the hub. This trend can

also be inferred from Equation (22) as noted by Lieblein and Ackley (Ref. 43) since at the casing and at the hub because of the boundary

$$V_r \equiv 0 \tag{32}$$

and hence

$$\frac{\partial(rV_\theta)}{\partial r} = 0. \tag{33}$$

Thus $|V_{\theta,2}|$ and β_2 must decrease from the specific or design value at the tip and increase at the hub as indicated qualitatively in Figure 21. It is the prediction of the over-turning and under-turning or the change in deviation angle which is of interest in this section.

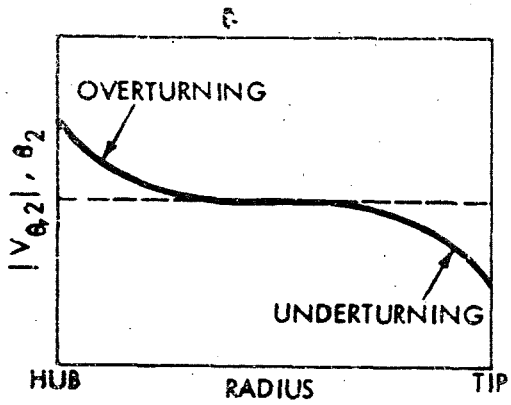

Figure 21 – Effect of mainstream, secondary flow in a cascade with spanwise increasing circulation.

Lieblein and Ackley (Ref. 43) have presented a method to compute the change in deviation angle due to the combined effects of cascade secondary flow and mainstream secondary flow for inlet guide vanes. They derived an approximate theoretical expression for the secondary velocities in the trailing edge plane containing a constant which was evaluated experimentally. The main flow was assumed to be irrotational and the blades were replaced by lifting lines or vortex bundles of strength equal to the blade circulation at each radius. For blades with radially varying circulation, vortex lines from the lifting line were assumed to trail downstream of the trailing edge forming a vortex sheet (Fig. 22). However, for some unexplained reason it was necessary to superimpose the induced velocities from a vortex system of magnitude equal to the trailing vortex sheet, but

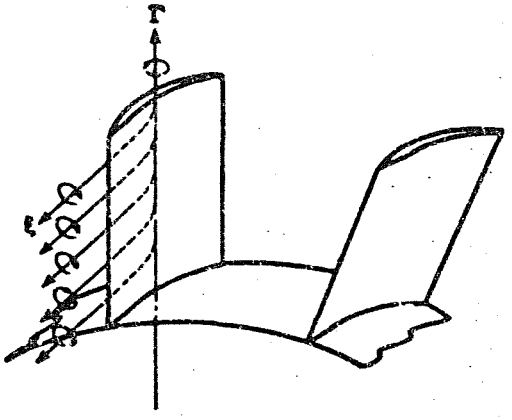

Figure 22 – Trailing vortex sheet.

to satisfy the boundary condition at the annulus walls. An additional vortex was located in the boundary layer region near each annulus wall to approximate the effects of cascade secondary flow (Fig. 23). The secondary flow velocity V_n induced normal to the streamline by all vortices from all blades in the cascade was calculated only on a radial line at the blade trailing edge rather than being averaged across the blade spacing at each radii. An experimental correction factor was applied to the resulting secondary flow induced turning angle (Fig. 24)

having opposite sign and from associated vortex images located outside the annulus on the blade element axisymmetric main flow to obtain an approximation to the actual radial variations of deviation angle. The vortex images shown in Figure 23 were required

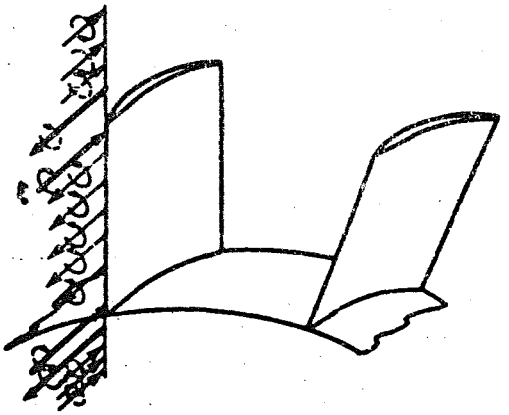

Figure 23 – Trailing vortex sheet and associated image vortices.

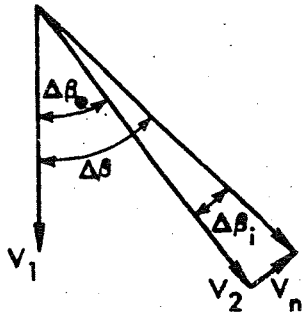

Figure 24 – Induced turning angle correction.

$$\Delta\beta_i = C \tan^{-1} \frac{V_n}{V_2}. \qquad (34)$$

Turning angles predicted using this theory were compared with experimental results for five compressor

guide vanes and one turbine nozzle. A satisfactory comparison resulted when a correction factor, C, of 0.42 was used.

Smith (Ref. 36) has presented a more general analysis considering frictionless, compressible flow with distributed vorticity (but no entropy gradients) for both rotating and stationary cascades. His analysis allows secondary velocities to be calculated for both cascade and mainstream secondary flows using the conventional axisymmetric solution as the basic flow. In an axisymmetric solution the flow through the cascade is assumed to remain on surfaces of revolution but as mentioned previously in real flow, due to what are defined as secondary velocities, the stream surfaces may be warped leading to a discontinuity of velocity at the blade trailing edge which creates a vortex sheet extending downstream from the blade. A major assumption of Smith's (Ref. 36) analysis is that the distortion of these stream surfaces is not large. A relation for the secondary streamwise vorticity in the flow at the trailing edge plane was derived with the aid of the vortex laws of fluid mechanics for a channel consisting of the axisymmetric stagnation streamlines and the two blade surfaces. The expression obtained is

$$\xi_s a = \left(V_1' \xi_{\perp,1} \frac{\Gamma_{VA}}{(V_\infty')^2} + \frac{d\Gamma_V}{dh_1}\right) \frac{dh_1}{dh_2} \tag{35}$$

where a is the distance between the exit streamlines (Fig. 25), V_1' is the inlet relative velocity, $\xi_{\perp,1}$ is the component of inlet vorticity normal to V_1', Γ_{VA} is the blade circulation in the actual flow (primary and secondary), V_∞' is the vector mean of the inlet and exit relative velocities, Γ_V is the blade circulation in the primary flow, and h_1 and h_2 are inlet and exit streamtube heights. Blade circulation is always considered positive and the secondary vorticity is considered positive when it induces secondary velocities on the suction surface which are in the positive h-direction. From Equation (35) ξ_s

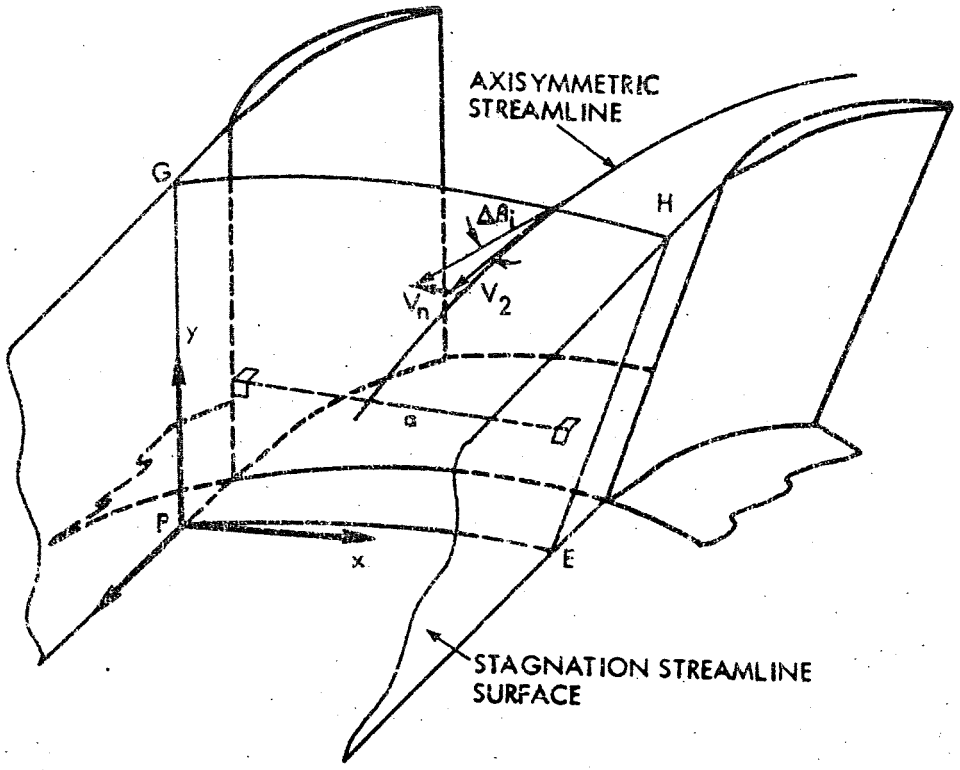

Figure 25 — Exit plane in which secondary flow is assumed to occur.

can be determined for all points in the exit flow.

It is assumed that the secondary velocities corresponding to ξ_s can be expressed as

$$\xi_s = \frac{\partial V_y}{\partial x} - \frac{\partial V_x}{\partial y} \tag{36}$$

where the x-y plane is normal to the stagnation streamline surfaces. That is, it was assumed that the secondary flow takes place in a plane bounded by the annulus walls and the exit axisymmetric stagnation streamline surfaces (Fig. 25). A secondary flow stream function was defined such that

$$\frac{\partial^2 \psi_s}{\partial x^2} + \frac{\partial^2 \psi_s}{\partial y^2} = \xi_s. \tag{37}$$

This equation was solved subject to the boundary conditions of ψ_s = constant on the boundary of a rectangle which approximated the surface EFGH shown in Figure 25. The details of the solution of this equation are not given in Reference 36 but they are given in Reference 44 together with the resulting equations necessary to find the average secondary tangential velocity. The equations are presented in graphical form in Reference 36 and 44 for aspect ratios of 1/π and 0.6/π, however for other aspect ratios the equations must be evaluated to obtain a value of the average secondary tangential velocity. The secondary velocity would then be superimposed on the axisymmetric solution to obtain the change in deviation angle (Fig. 25).

Tip Clearance Leakage Flow

Leakage flow through the clearance gap between the end of a blade and an annulus wall (Fig. 26) tends to decrease the difference in pressure between

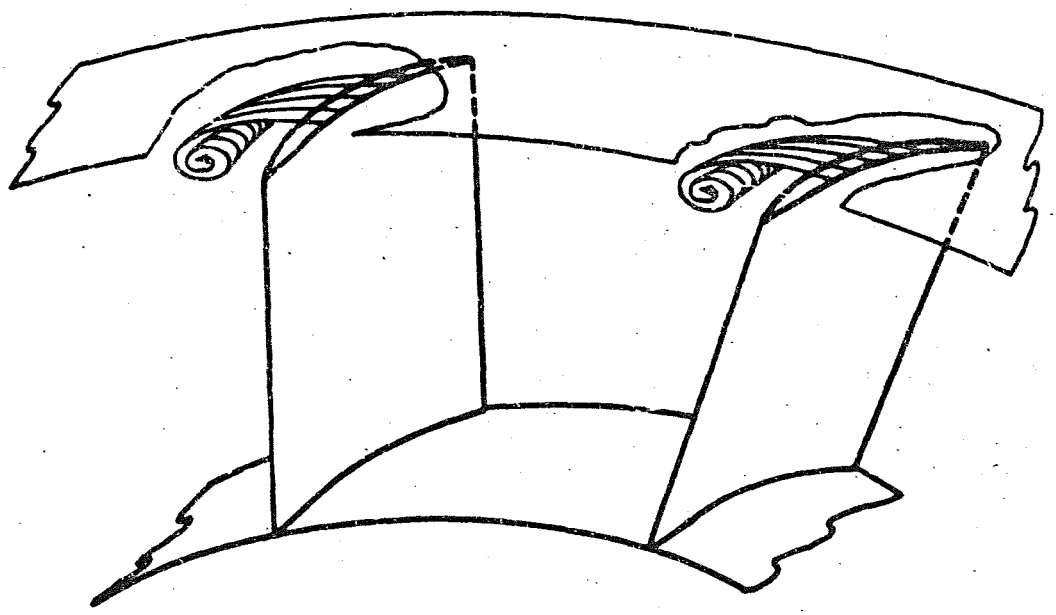

Figure 26 – Leakage flow.

the suction and pressure surfaces of the blade sections near the gap. The flow around the sections near the tip is turned through a smaller angle on the average (i.e. the deviation angle is larger) than it would be if no leakage flow existed. The actual flow field near the clearance gap is complicated by the interaction of the leakage flow and the three-dimensional annulus-wall boundary layer flow which was described in the section on cascade secondary flow.

Lakshiminarayana and Horlock (Ref. 40) have developed an approximate theoretical method to obtain the change in deviation angle caused by the leakage flow in a stationary cascade. They assumed the flow to be steady, inviscid, and incompressible. The flow model assumed that the leakage flow caused the actual blade element circulation to decrease only partially from the two-dimensional circulation. The decrease in circulation was assumed to be $(1 - K)\Gamma_{2D}$ (where K is the fraction of lift retained at the tip) and was treated as trailing vorticity distributed between the blades from the wall to the edge of the boundary layer as indicated in Figure 27.

The strength of the vorticity was assumed to be constant from blade-to-blade, but to vary sinusoidally in the spanwise direction increasing from zero at the wall to a maximum at $\delta_1/2$ from the wall and then decreasing to zero at the edge of the boundary layer.

$$\xi_c = (\xi_c)_{max} \sin \frac{\pi x}{\delta_1} . \tag{38}$$

A stream function was defined for the leakage secondary flow which satisfied

$$\nabla^2 \psi_c = \xi_c \qquad 0 < x < \delta_1 \tag{39}$$

$$\nabla^2 \psi_c = 0 \qquad x > \delta_1 \tag{40}$$

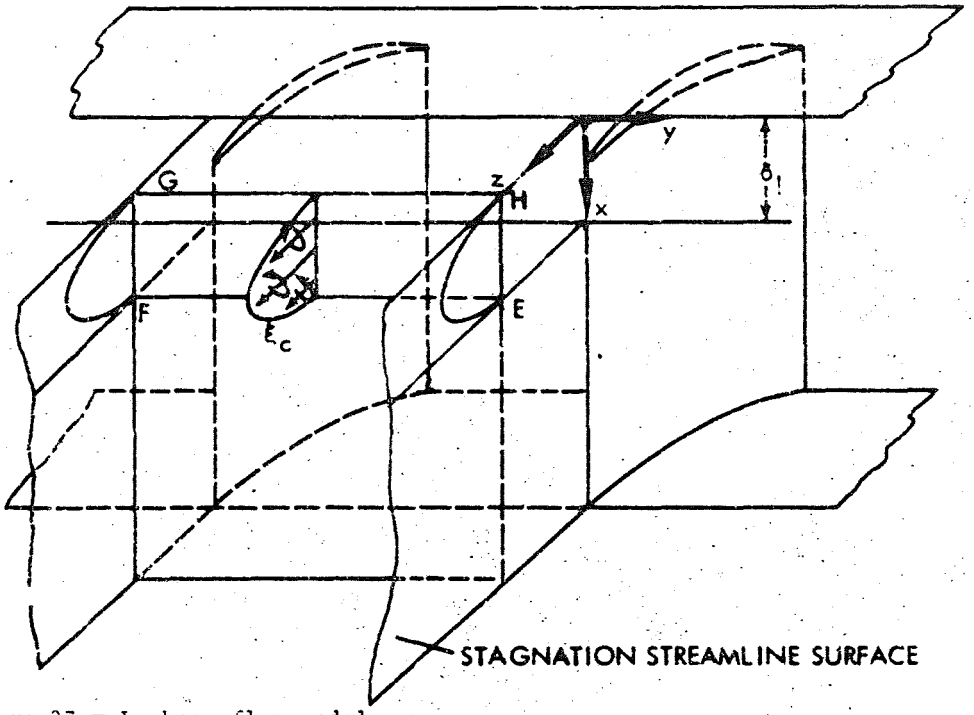

Figure 27 – Leakage flow model.

and $\xi_c = 0$ on the boundary EFGHE in Figure 27. The change in the average outlet angle (also the change in deviation angle) was shown to be

$$(\Delta\bar{\beta}_2) = \frac{2}{\pi V_2} \sum_{j=1}^{\infty} \frac{\xi'_{c,j}}{j} \tag{41}$$

where

$$\xi'_{c,j} = \frac{-4\,(\xi_c)_{max}\,\delta_1}{j\pi^2\left[1 + \left(j\,\frac{\delta_1}{s\cos\beta_2}\right)\right]} \left\{ \frac{\sinh\left(\frac{j\pi\delta_1}{s\cos\beta_2}\right)}{\sinh\left(\frac{j\pi\ell}{s\cos\beta_2}\right)} \cosh\left[\frac{j\pi\ell}{s\cos\beta_2}\left(1 - \frac{z}{\ell}\right)\right] \right\}. \tag{42}$$

Theoretical predictions of the change in the average outlet angle using an experimental value of K were compared with experimental data from a rectilinear cascade of 10C430C50 profile blades having a 36 degree blade setting angle. The tip clearance gap was simulated by a gap at midspan and a wake was generated upstream to simulate the annulus wall boundary layer. The cascade

secondary flow angle changes were computed using the theory of Louis (Ref. 45) and were superimposed directly on the changes due to leakage flow. Quantitative agreement between theory and experimental data was closest near the blade tip with the discrepancy increasing to about 2 degrees near the edge of the wake.

SWEEP AND DIHEDRAL

The term sweep is applied to turbomachinery blades when the flow direction is not perpendicular to the spanwise direction and the sweep angle, λ, is defined in Figure 28. A turbomachine blade has a nonzero dihedral angle, ν, whenever

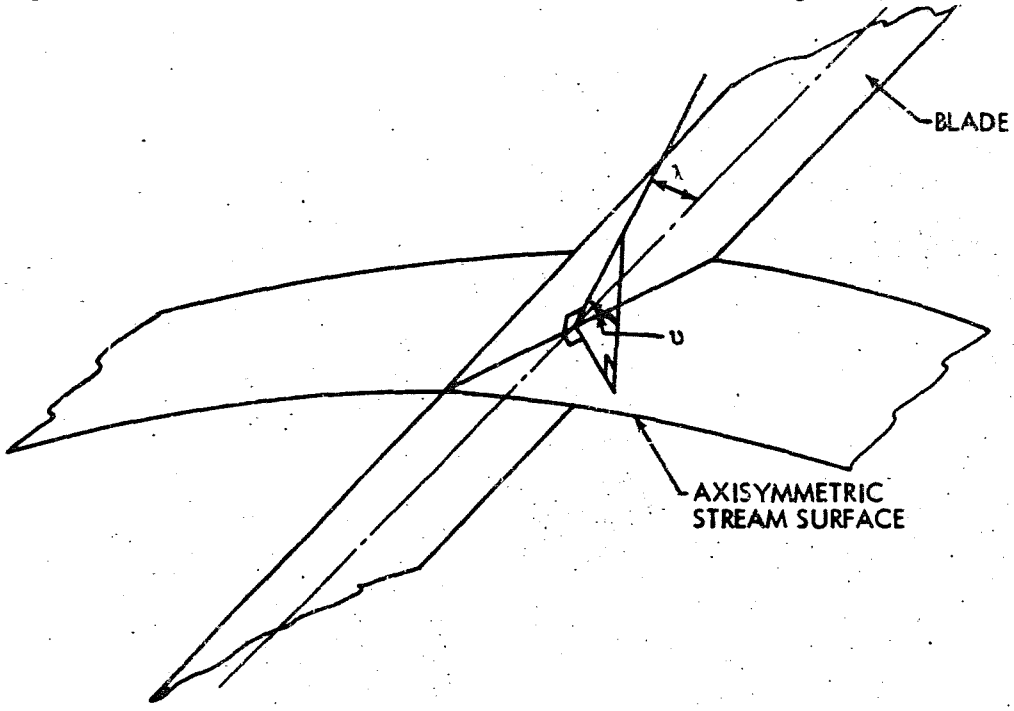

Figure 28 — Blade with sweep and dihedral.

the intersection of an axisymmetric stream surface and the blade surface is not perpendicular (see Fig. 28). Smith and Yeh (Ref. 46) have given a numerical example which shows that applying two-dimensional cascade deviation angles to the geometry of view A-A, Figure 29 gives too large a deviation

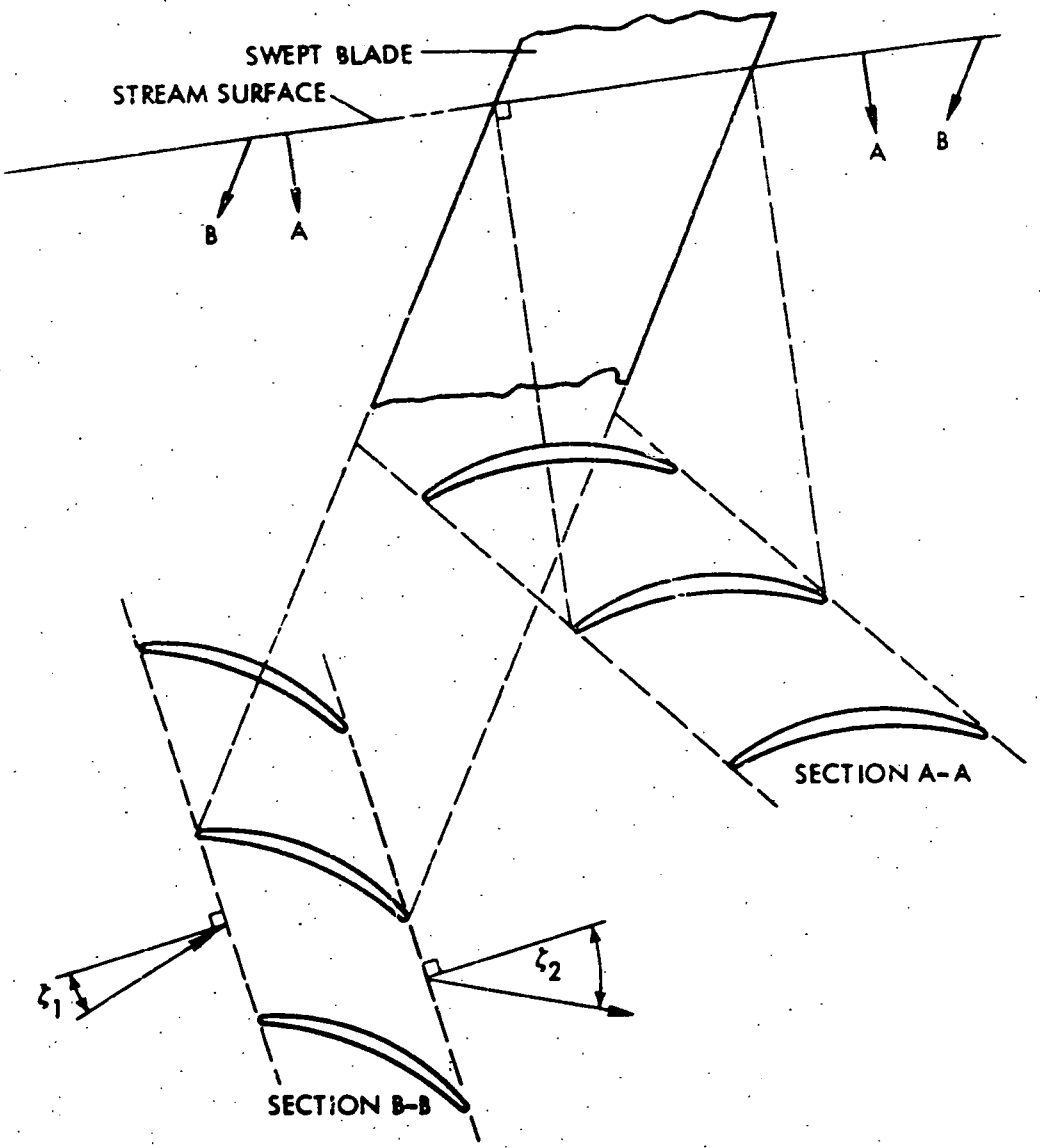

Figure 29 — Two views of blade sections of a swept blade.

angle for a cascade with an infinite span in inviscid, steady flow. They show that the correct deviation angle is obtained by viewing the flow along

a line parallel to the blade axis, applying two-dimensional cascade data to the corresponding cascade (view B-B, Fig. 29), and projecting the flow angles in view B-B back into the cascade of view A-A, Figure 29. The same method is recommended for use on blades with dihedral. Smith and Yeh (Ref. 46) have developed relationships which can be used to account for the effect of sweep and dihedral angle on deviation angle in the design problem. The basic effects are incorporated by projecting the flow angles from the axisymmetric design solution onto surfaces which are normal to the blade axis. The flow angle in the normal stream surface is given by

$$\tan \zeta = \frac{\tan \beta - \cos \mu \tan \tau \,(\cos \mu \tan \alpha + \sin \mu)}{(\cos \mu - \sin \mu \tan \alpha)\sqrt{1 + \cos^2 \mu \tan^2 \tau}} \qquad (43)$$

where $\alpha = \arctan (V_r/V_z)$, $\beta = \arctan (V_\theta/V_z)$, and where μ, τ, and ζ are defined in Figures 29 and 30. Equations are also

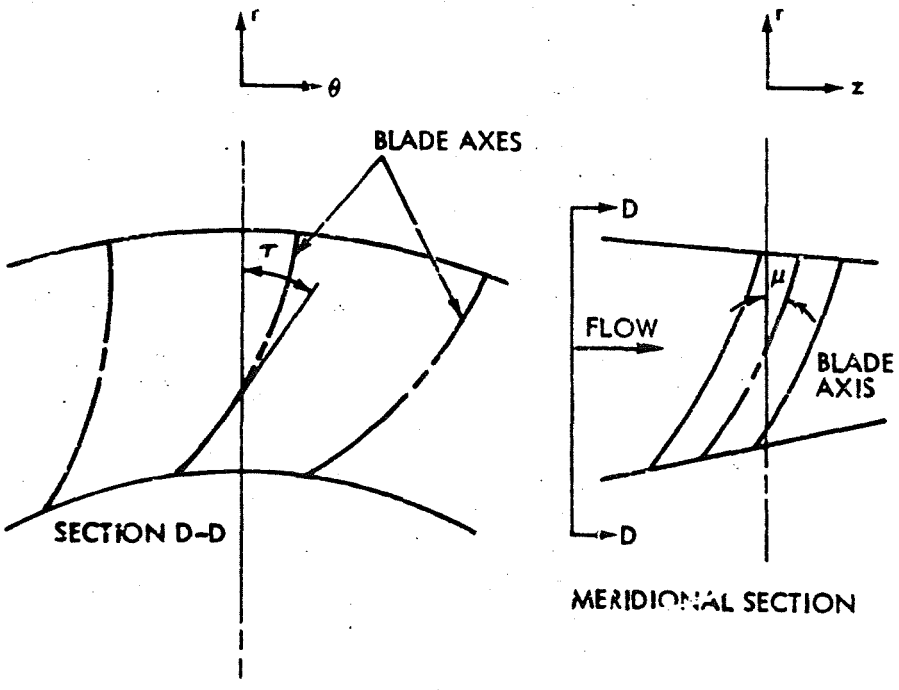

Figure 30 — Annular cascade of blades with sweep and dihedral.

given for the determination of the sweep and dihedral angles. Blade sections corresponding to view B-B of Figure 29 can then be obtained using two-dimensional cascade data and the flow angles ζ from Equation (43). The angle ζ obtained from Equation (43) is appropriate only for a blade with an infinite span, thus a correction for the effect of the annulus end walls is required. Smith and Yeh (Ref. 46) developed an approximate correction in the form of a downwash or induced tangential velocity which attains a maximum value at the annulus walls and decays to zero at some distance from the wall. For the special case of elliptical loading (circular-arc camber line) along the chord a polynomial equation was presented for the downwash velocity at the wall and additional equations permit computation of the spanwise locations where the downwash velocity has decayed to 0.5 and 0.1 of the maximum magnitude. Smith and Yeh (Ref. 46) recommend obtaining an axisymmetric solution at several stations within the blade row as well as upstream and downstream. Equation (43) can then be used to obtain the flow angle ζ at several points along the chord. It is not clear, however, how cascade data can be applied within the blade row to obtain blade angle as a function of chord unless some chordwise distribution of deviation angle is assumed. If the chordwise distribution of deviation angle is known then it can be readily corrected for endwall effects using Smith and Yeh's (Ref. 46) results and the design blade angles projected into the surface normal to the blade axis can be computed from ζ and δ. Blade profiles on cylindrical surfaces or other surfaces must be obtained by application of descriptive geometry.

No similar treatment of the effects of sweep and dihedral has been formulated for the off-design or analysis problem although the design method of Smith and Yeh (Ref. 46) could be adapted to the analysis problem.

Experimental investigations of the effect of sweep angle have been

conducted by Beatty, et al. (Ref. 47), Murai, et al. (Ref. 48), and Stark (Ref. 49) using plane cascades and by Godwin (Ref. 50) using a rotor. However no empirical methods for predicting the effect of sweep on deviation angle have been proposed on the basis of these limited results.

SUMMARY

Methods of predicting deviation angles on a blade element basis in axial-flow pumps and compressors were reviewed. The effect of two-dimensional geometric parameters on deviation angle may be accounted for with the methods of Carter and Hughes (Ref. 3) and Lieblein (Ref. 2). Smith (Ref. 11) and Lieblein (Ref. 9). have presented corrections to obtain deviation angles over a range of incidence angles. Corrections for axial velocity ratio in rectilinear cascades may be based on the velocity diagram methods of Erwin and Emery (Ref. 16) or the potential flow analyses of Shaalan and Horlock (Ref. 26) and Kubota (Ref. 27).

Smith (Ref. 36) presents the most general approach to correct deviation angle for the effects of cascade and mainstream secondary flow. Lakshiminarayana and Horlock (Ref. 40) have developed a correction for the change in deviation angle due to tip clearance leakage flow in a plane cascade. A method of correcting deviation angle for the effects of blade sweep and dihedral in the design problem is given by Smith and Yeh (Ref. 46).

RECOMMENDATIONS FOR FUTURE RESEARCH

An extension of the two-dimensional cascade tests reported in Reference 7 to higher cambers would provide a significant contribution to axial-flow pump technology. As indicated in the Two-Dimensional Geometric Parameters Section, at high values of camber where the D-factor is greater than 0.62, deviation angle appears to become a nonlinear function of camber. This nonlinear tendency should be clarified experimentally.

The effect of nonconstant axial velocity through a cascade is of considerable interest since in general the axial velocity ratio in a real machine is not equal to one. A systematic study in a plane cascade in which axial velocity ratio could be varied over a wide range could produce fundamental results in this area. A thorough comparison of the experimental results with potential flow solutions would contribute toward the establishment of the applicability and accuracy of the potential flow solutions. The validity of applying two-dimensional axial velocity ratio corrections to annular cascades also deserves study to determine how important the chordwise distribution of local axial velocity ratio is in determining the deviation angle for a given value of the overall axial velocity ratio.

ACKNOWLEDGMENTS

The guidance and help given to the author by Professor George K. Serovy during the preparation of this review is gratefully acknowledged. Appreciation is also expressed for the support given to the Engineering Research Institute by the National Aeronautical and Space Administration through Grant NGL 16-002-005.

JW/lmc

REFERENCES

1. Serovy, George K., "Utilization of Cascade Data in Axial-Flow Compressor Design and Analysis — A Critical Review," Iowa State University, Engineering Research Institute, Ames, Iowa. Preprint ERI 555. 1969.

2. Lieblein, Seymour, "Experimental Flow in Two-Dimensional Cascades," in Johnsen, Irving A. and Bullock, Robert O., eds. Aerodynamic Design of Axial-Flow Compressors, U. S. National Aeronautics and Space Administration Special Publication 36. pp. 183-226. 1956.

3. Carter, A. D. S. and Hughes, Hazel P., "A Theoretical Investigation Into the Effect of Profile Shape on the Performance of Aerofoils in Cascade," Aeronautical Research Council Reports and Memoranda No. 2384. 1946.

4. Carter, A. D. S., "The Low Speed Performance of Related Aerofoils in Cascades," Aeronautical Research Council Current Papers No. 29. 1950.

5. Howell, A. R., "The Present Basis of Axial Flow Compressor Design. Part 1. Cascade Theory and Performance," Aeronautical Research Council Reports and Memoranda No. 2095. 1942.

6. Constant, H., "Performance of Cascades of Aerofoils," Unpublished document. Aeronautical Research Council No. 4155. 1939.

7. Emery, James C., Herrig, L. Joseph, Erwin, John R., and Felix, A. Richard, "Systematic Two-Dimensional Cascade Tests of NACA 65-series Compressor Blades at Low Speeds," U. S. National Advisory Committee for Aeronautics Report 1368. 1958.

8. Lieblein, Seymour, Schwenk, Francis C., and Broderick, Robert L., "Diffusion Factor for Estimating Losses and Limiting Blade Loadings in Axial-Flow-Compressor Blade Elements," U. S. National Advisory Committee for Aeronautics Research Memorandum E53D01. 1953.

9. Lieblein, Seymour, "Incidence and Deviation-Angle Correlations for Compressor Cascades," American Society of Mechanical Engineers Trans. Series D: Journal of Basic Engineering 82:575-584. 1960.

10. Weinig, Fritz, "Die Stromung un die Schauflen von Turbomachinen," Johann Ambrosius Barth, Leipzig. 1935.

11. Smith, Leroy H., Jr., "Discussion," American Society of Mechanical Engineers Trans. Series D: Journal of Basic Engineering 82:585-596. 1960.

12. Abbott, Ira H., Von Doenhoff, Albert E., and Stivers, Louis S., Jr., "Summary of Airfoil Data," U. S. National Advisory Committee for Report No. 824. 1945.

13. Howell, A. R., "Flow in Cascades," in Hawthorne, W. R., ed. High Speed Aerodynamics and Jet Propulsion, Vol. 10, Aerodynamics of Turbines and Compressors. Princeton Univ. Press, Princeton. New Jersey. 1964.

14. Miller, Max J., and Sandercock, Donald M., "Blade Element Performance of Axial-Flow Pump Rotor with Blade Tip Diffusion Factor of 0.66," U. S. National Aeronautics and Space Administration Technical Note D-3602. 1966.

15. Katzoff, S., Bogdonoff, Harriet E., and Boyet, Howard, "Comparisons of Theoretical and Experimental Lift and Pressure Distributions on Airfoils in Cascade," U. S. National Advisory Committee for Aeronautics Technical Note 1376. 1947.

16. Erwin, John R., and Emery, James C., "Effect of Tunnel Configuration and Testing Technique on Cascade Performance," U. S. National Advisory Committee for Aeronautics Report 1016. 1951.

17. Pollard, D. and Costelow, J. P., "Some Experiments at Low Speed on Compressor Cascades," American Society of Mechanical Engineers Trans., Series A: Journal of Engineering for Power. 89:427-436. 1967.

18. Montgomery, S. R., "Spanwise Variations of Lift in Compressor Cascades. Part 1. Experiments." Journal of Mechanical Engineering Science 1:293-304. 1959.

19. Montgomery, S. R., "Three-Dimensional Flow in Compressor Cascade," Mass. Inst. Tech. Gas Turbine Lab. Report No. 48. 1958.

20. Heilmann, W., "Experimentelle und grenzschichttheoretische Untersuchungen an ebenen Verzögerungsgittern bei kompressibler Strömung, insbesondere bei Änderung des axialen Stromdichteverhältnisses und der Zuströmturbulenz," Deutsche Luft - und Raumfahrt Forschungsbericht 67-88. 1967.

21. Heilmann, W., Starken, H., and Weyer, H., "Cascade Wind Tunnel Tests on Blades Designed for Transonic and Supersonic Compressors," Advisory Group for Aerospace Research and Development Conf. Proc. No. 34:12-1 - 12-16. 1968.

22. Savage, Melvyn, Felix, A. Richard, and Emery, James C., "High-Speed Cascade Tests for a Blade Section Designed for Typical Hub Conditions of High-Flow Transonic Rotors," U. S. National Advisory Committee for Aeronautics Research Memorandum L55F07. 1955.

23. Scholz, N., "Two-Dimensional Correction of the Outlet Angle in Cascade Flow," Journal of the Aeronautical Sciences, Readers Forum, 20:786-787. 1953.

24. Pollard, D., and Horlock, J. H., "A Theoretical Investigation of the Effect of Change in Axial Velocity on the Potential Flow Through a Cascade of Aerofoils," Aeronautical Research Council Current Papers No. 619. 1963.

25. Mani, R. and Acosta, A. J., "Quasi Two-Dimensional Flows Through A Cascade," American Society of Mechanical Engineers Paper 67-WA/FE-9. New York. The Society. 1966.

26. Shaalan, M. R. A. and Horlock, J. H., "The Effect of Change in Axial Velocity on the Potential Flow in Cascades," Aeronautical Research Council Reports and Memoranda No. 3547. 1968.

27. Kubota, Shigeo, "Cascade Performance with Accelerated or Decelerated Axial Velocity," Japan Society of Mechanical Engineers Bulletin 5:450-460. 1962.

28. Pollard, D., and Wordsworth, J., "A Comparison of Two Methods for Predicting the Potential Flow Around Arbitrary Airfoils in Cascade," Aeronautical Research Council Current Papers No. 618. 1962.

29. Mellor, G. L., "An Analysis of Axial Compressor Cascade Aerodynamics," American Society of Mechanical Engineers Trans., Series D: Journal of Basic Engineering 81:362-378. 1959.

30. Mani, R., "A Method of Calculating Quasi Two-Dimensional Flows Through Cascades," California Institute of Technology Engineering Report No. E-79.10. 1967.

31. Schulze, Wallace M., Erwin, John R., and Ashby, George C., "NACA 65-series Compressor Rotor Performance with Varying Annulus-Area Ratio, Solidity, Blade Angle, and Reynolds Number and Comparisons with Cascade Results," U. S. National Advisory Committee for Aeronautics Technical Note 4130. 1957.

32. Jansen, W. and Moffatt, W. C., "The Off-Design Analysis of Axial-Flow Compressors," American Society of Mechanical Engineers Trans., Series A: Journal of Engineering for Power 89:453-462. 1967.

33. Herzig, Howard Z., Hansen, Arthur G., and Costello, George R., "A Visualization Study of Secondary Flows in Cascades," U. S. National Advisory Committee for Aeronautics Report 1163. 1954.

34. Louis, Jean F., "Secondary Flow and Losses in a Compressor Cascade," Aeronautical Research Council Reports and Memoranda No. 3136. 1958.

35. Rohlik, Harold E., Kofskey, Milton G., Allen, Hubert W., and Herzig, Howard Z., "Secondary Flows and Boundary-Layer Accumulations in Turbine Nozzles," U. S. National Advisory Committee for Aeronautics Report 1168. 1954.

36. Smith, L. H., Jr., "Secondary Flow in Axial-Flow Turbomachinery," American Society of Mechanical Engineers Trans. 77:1065-1076. 1955.

37. Lakshminarayana, B. and Horlock, J. H., "Review: Secondary Flows and Losses in Cascades and Axial-Flow Turbomachines," International Journal of Mechanical Sciences 5:287-307. 1963.

38. Hawthorne, W. R., "Secondary Circulation in Fluid Flow," Royal Society of London, Proc. 18:374-387. 1951.

39. Lakshminarayana, B. and Horlock, J. H., "Effect of Shear Flows on the Outlet Angle in Axial Compressor Cascades — Methods of Prediction and Correlation with Experiments," American Society of Mechanical Engineers Trans., Ser. D 89:191-200. 1967.

40. Lakshminarayana, B. and Horlock, J. H., "Leakage and Secondary Flows in Compressor Cascades," Aeronautical Research Council Reports and Memoranda No. 3483. 1967.

41. Soderberg, Olof, "Secondary Flow and Losses in a Compressor Cascade," Mass. Inst. of Tech. Gas Turbine Lab. Report No. 46. 1958.

42. Vavra, M. H., Aero-Thermodynamics and Flow in Turbomachines, John Wiley and Sons, New York. c1960.

43. Lieblein, Seymour and Ackley, Richard H., "Secondary Flows in Annular Cascades and Effects on Flow in Inlet Guide Vanes," U. S. National Advisory Committee for Aeronautics Research Memorandum E51G27. 1951.

44. Smith, Leroy H., Jr., "Three-Dimensional Flow in Axial-Flow Turbomachinery," Wright Air Development Center Technical Report 55-348 Vol. 1. 1955.

45. Louis, Jean F., "Rotational Viscous Flow," International Congress for Applied Mechanics, 9th, Brussels, 1956, Proc. 3:306-317. 1957.

46. Smith, Leroy H., Jr. and Yeh, Hsuan, "Sweep and Dihedral Effects in Axial-Flow Turbomachinery," American Society of Mechanical Engineers Trans., Series D 85:401-414. 1963.

47. Beatty, Loren A., Emery, James C., and Savage, Melvyn, "Low-Speed Cascade Tests of Two 45° Swept Compressor Blades with Constant Spanwise Loading," U. S. National Advisory Committee for Aeronautics Research Memorandum L53L07. 1954.

48. Murai, H., Hirata, Y., and Mikashima, Y., "Research on Swept-Back Blades Laid Between Parallel Walls, Report 1 (Experimental Research on Clark Y 11.7% Blade with Aspect Ratio of 2.0)," Sendai, Japan, Tohuku Univ., Institute of High Speed Mechanics, Report 17:185-231. 1966.

49. Stark, Udo, "Flow Investigations Around Swept Compressor Cascades at Compressible Subsonic Flow," Deutsche Forschungsanstalt fur Luft-und Raumfahrt DFL-0331. 1966.

50. Godwin, William R., "Effect of Sweep on Performance of Compressor Blade Sections as Indicated by Swept-Blade Rotor, Unswept-Blade Rotor, and Cascade Tests," U. S. National Advisory Committee for Aeronautics Technical Note 4062. 1957.

SYMBOLS

A	annulus area, ft^2
a	distance between exit stagnation streamlines, in. (Fig. 25)
AVR	axial velocity ratio, $V_{z,2}/V_{z,1}$
b	plane located between leading and trailing edge of cascade (Fig. 12)
C	empirical correction factor
c	chord, in. (Fig. 3)
C_{L_0}	isolated airfoil lift coefficient at design angle of attack
C_p	coefficient of pressure, $(p - p_1)/\frac{1}{2}\rho V_1^2$
D	diffusion factor, $D = 1 - \frac{V_2'}{V_1'} \pm \frac{r_2 V_{\theta,2}' - r_1 V_{\theta,1}'}{(r_1 + r_2)\sigma V_1'}$ (+ rotor, - stator)
d	tangential velocity increase, ft/sec (Fig. 10)
f	function, $-\frac{1}{x}\left(\frac{\partial \phi}{\partial x}\right)$ (Eq. 11)
g	force-mass conversion factor, 32.174 lb_m ft/lb_f sec^2
h	streamtube height, in.
i	incidence angle, deg. (Fig. 3)
j	index of summation
K	fraction of lift retained at tip
k	constant (Eq. 9)
$(K_\delta)_{sh}$	blade shape correction factor
$(K_\delta)_t$	blade thickness correction factor
ℓ	blade span, in.
M	Mach number
m	slope factor (Eq. 3)
m_c	slope factor in Carter's rule
n	number of blades

P	total pressure, psia
p	static pressure, psia
Q	mass rate of flow, $ft.^3/sec$
r	radius, ft.
R_c	streamline radius of curvature, ft.
Re	blade chord Reynolds number
s	blade spacing, in. (Fig. 3)
t	blade thickness, in.
u	induced velocity normal to streamline, ft/sec
V	fluid velocity, ft/sec
w	induced velocity in the spanwise direction, ft/sec
x	coordinate direction
z	coordinate direction
α	slope of streamline in meridional plane, arctan (V_r/V_z), deg.
β	flow angle, angle between flow and axial direction, deg.
Γ	blade circulation (Eq. 6)
γ	blade stagger angle, angle between chord line and axial direction, deg (Fig. 3)
δ	deviation angle, deg. (Fig. 3)
δ_o	reference deviation angle for zero camber, deg.
$(\delta_o)_{10}$	reference zero camber deviation angle for NASA 65-series blade section with $t_{max}/c = 0.10$, deg.
δ_1	boundary layer thickness, in.
$\delta_{AVR=1.0}$	deviation angle for plane, two-dimensional cascade flow (AVR = 1), deg.
ϵ	flow turning angle $\beta_1' - \beta_2'$, deg.
ζ	flow angle projected onto the stream surface normal to the blade leading edge, deg.
η	angle between the normal to the Bernoulli surface and principal normal to streamline, deg. (Fig. 17)

θ coordinate in tangential direction

κ blade angle, angle between tangent to blade mean camber line and axial direction, deg. (Fig. 3)

λ sweep angle, deg. (Fig. 28)

μ projection of λ into meridional plane, deg. (Fig. 30)

ν dihedral angle, deg. (Fig. 28)

ξ streamwise component of vorticity, sec^{-1}

ξ_1 component of vorticity normal to streamline, sec

ρ fluid density, lb_m/ft^3

τ angle between blade axis and radial direction projected into r - θ plane, deg. (Fig. 30)

τ angle of attack

σ blade solidity, c/s

ϕ velocity potential

ϕ^o blade camber angle, $\kappa_1 - \kappa_2$, deg. (Fig. 3)

ψ stream function

ω axial velocity density ratio

$\bar{\omega}$ total pressure loss coefficient, $\dfrac{P_{2,id}' - P_2'}{P_1' - P_1}$

Subscripts

b plane b (Fig. 12)

c leakage secondary flow

cor corrected

e blade element

i induced by secondary flow

id ideal

j summation index

m mean

max maximum

min minimum

n component of secondary flow normal to streamline and tangent to the axisymmetric stream surface, (Fig. 25)

nom	at nominal incidence angle
r	radial direction
ref	reference (Fig. 6)
s	secondary flow
v	primary flow
VA	actual flow
x	x-coordinate direction
y	y-coordinate direction
z	axial direction
θ	tangential direction
1	cascade inlet
2	cascade outlet
2D	two-dimensional
∞	vector mean of inlet and outlet value

Superscripts

'	relative to moving blade
$\bar{}$	circumferential average
$\vec{}$	vector quantity
$\hat{}$	average over streamtube

APPENDIX – CASCADE CONFIGURATION VARIABLES AND FLOW PARAMETERS

Starred items* in these tables are significant only when cascade flow is not two-dimensional (uniform entrance conditions, exit/entrance density-axial velocity ratio = 1.0).

TABLE 1 – CASCADE CONFIGURATION VARIABLES

BLADE SECTION GEOMETRY

- Camber Line Form
  - Chordwise location of maximum camber
  - Value of maximum camber (or camber angle)
- Basic Profile Form
  - Chordwise distribution of profile thickness
    - $\frac{\text{maximum thickness}}{\text{chord length}}$ ratio value
  - Leading-edge radius
  - Trailing-edge radius or thickness
- Manufacturing Tolerances
  - Profile errors
    - individual coordinate
    - surface contour waviness
  - Surface finish

BLADE CHORD ANGLE = STAGGER ANGLE

SOLIDITY

MISCELLANEOUS CASCADE GEOMETRY

- Blade Leading-Edge Sweep
- Blade Aspect Ratio*
- Spanwise Blade Section Variation* } Annular cascade
  - Blade twist* }
- Dihedral
- Tip Clearance*

- Row Spacing in Direction Perpendicular to Leading-Edge Plane } Tandem cascades
- Relative Orientation of Rows in Direction Tangential to Leading-Edge Plane }

FLOW CONTROL SYSTEMS

- Variable-Geometry Blading
  - Flaps
  - Slots
- Boundary-Layer Control
  - Suction
  - Blowing

TABLE 2 — CASCADE FLOW PARAMETERS — INDEPENDENT VARIABLES

THERMODYNAMIC PROPERTY CHARACTERISTICS OF WORKING FLUID

- Entrance Total Pressure and Temperature
- Fluid Specific Heat Ratio

ENTRANCE FLOW CHARACTERISTICS

- Entrance Mach Number
- Cascade Reynolds Number
- Spanwise Distribution of Entrance Velocity (Shear Flow)*
- Time Variation in Entrance Velocity and Flow Angle
  - Magnitude of variation
  - Frequency of variation
  - Form of variation (time profile)

ENTRANCE TURBULENCE CHARACTERISTICS

- Intensity
- Scale
- Isotropy

INCIDENCE ANGLE

CASCADE DENSITY x AXIAL VELOCITY RATIO*